Spectral Properties of the Dimerized Fermi Hubbard Model

von Karin Haderlein

Masterarbeit in Physik

angefertigt im
Physikalischen Institut

vorgelegt der
Mathematisch-Naturwissenschaftlichen Fakultät
der
Rheinischen Friedrich-Wilhelms-Universität
Bonn

März 2023

I hereby declare that the work presented here was formulated by myself and that no sources or tools other than those cited were used.

Bonn, 02.03.2023 signature Karin Haderlein

1. Supervisor: Prof. Dr. Corinna Kollath
2. Supervisor: Prof. Dr. Hartmut Monien

Contents

1 Introduction

Understanding properties of materials has always been a major goal of research like gaining insight into high temperature superconductivity. In general, a full description of a material is too complex to solve or simulate due to various factors, for example the interaction strength of all particles. Thus, it is necessary to find simplified models which are still able to capture the relevant properties and dynamics.

A very well known basic model is given by the Hubbard model. In its most simplified form, it consists of a sinusoidal potential where we associate the minima of the potential with lattice sites. It is possible to consider fermions or bosons in this lattice where we restrict ourselves to the fermionic case which respects the Pauli exclusion principle. The model considers only the possibility for the particles to hop to a neighbouring site, or to interact with a particle of opposite spin on the site.

While the concept of the Fermi Hubbard model is simple, it still captures interesting properties, e.g. Mott insulating and superfluid phases [Ess10] as well as topological dynamics [Nak+16]. In the latter, the topological transport is realised by periodically changing the parameters of the potential. Then, we do not directly encounter the simple Fermi Hubbard model but two extensions of it. These extensions are given by the ionic Hubbard model and the dimerized Hubbard model and consist of alternating on-site potentials or alternating hopping amplitudes.

Much research was already put into the Fermi Hubbard model. Specifically, in one dimension it has been shown to be Bethe ansatz solvable [LW68]. Thus, in this case it is understood as an integrable model. For the extensions of the Hubbard model such a classification by finding a solution to the model was not possible yet.

The question whether a model is integrable or not is of interest to understand its dynamical properties. For instance, one open problem in particular is the question of thermalization. It is assumed that chaotic models thermalize while integrable models do not [Sre94; RS12; RDO08; Rig09; DAl+16; NH15]. Moreover, we find different spectral properties for both chaotic and integrable models [BT77; Meh04]. This poses a link between spectral and dynamical properties of a system. Examining the properties of the level statistics is a useful and well developed tool for such an analysis [BT77; Wig55; Meh04; BGS84; Poi+93; OH07; Ata+13].

An analysis of the level statistics for the ionic Hubbard model has already been conducted, with a first result of it being integrable [HJ20]. This was later refuted [De +22] and now we expect the model to exhibit the spectral properties of a chaotic system. Until now, a similar analysis has not been conducted for the dimerized Hubbard model which is going to be the topic of the following thesis.

We start in section 2 with an introduction into the necessary theoretical background of chaotic and integrable systems as well as the meaning of level statistics. Moreover, we discuss the model and its symmetries. In section 3 we deal with the numerical procedure of generating a spectrum of the dimerized Hubbard model divided in symmetry subsectors. The analysis of the properties of the dimerized Hubbard models level statistics is the topic of section 4. We are going to examine the distribution of consecutive level spacing ratios in dependence on different parameters of the model as well as make a short comparison with the results of the ionic Hubbard

model. In the final section 5 we give a summary and come to a conclusion. Moreover, a short outlook is given.

2 Theoretical Background

Before we are able to begin with an analysis of the properties of the level statistics we are going to give an introduction into several parts of the theoretical background. First, we discuss the defining features of chaotic and integrable systems. Furthermore, we are going to motivate the link between chaos and integrability and thermalization. The level statistics are introduced as a method to examine whether a model shows chaotic or integrable nature. Moreover, since the level statistics require understanding of the underlying symmetries, we discuss the Fermi Hubbard model and its extensions with their known symmetries.

2.1 Chaotic and Integrable Systems

For a general introduction into the topic of quantum chaotic and integrable systems as well as thermalization we refer to [DAl+16; NH15].

Chaos and integrability accompany us throughout our studies of theoretical physics, beginning in classical mechanics. However, in quantum systems we have to find other approaches, as e.g. the exact position in space is replaced by a probability. Therefore, we should have a more detailed look at the defining properties of chaotic and integrable systems in quantum systems.

An essential part of integrability is given by the symmetries present. In classical mechanics we consider a system with N degrees of freedom. Then we can find N independent conserved quantities $Q_1, \dots, Q_N$. Here, the independence is meant in terms of Poisson brackets. These conservation laws result in a solution of the system [Arn89; Wim22].

An example of this is given by a particle in a two dimensional circle [DAl+16]. Here, we have both spatial coordinates as degrees of freedom. Additionally to the energy conservation we can find for this example the conservation of the angular momentum.

Now transferring to quantum mechanics, we can follow a similar approach. For our purposes it suffices to define an integrable quantum system by finding an extensive amount of symmetries yielding conserved quantities even though the rigorous definition is up to debate [CM11; Wei92]. Moreover, a model being integrable mostly corresponds to a model being solvable, e.g. by Bethe Ansatz [Ret22].

In contrast (quantum) choatic systems as the counterpart to integrable systems, do not exhibit this amount of symmetries. We can observe this in the classical limit considering the example of a two dimensional box. By adding a circle into the square box at which the particle can reflect, the system turns into a chaotic one. This is a representation of the so called Sinai billiard [Sin70] which is, as well as the Bunimovich stadium [Bun79], widely used as an example.

An important approximation of chaotic quantum systems is given by random matrix theory. The idea of random matrix theory was introduced by Wigner [Wig55] in relation to heavy nuclei resonances. The concept later proved to fit very well with results from chaotic quantum systems with a classical limit like the quantum Sinai

billiard and it is conjectured that the spectral properties of general quantum chaotic systems fit the expectations of random matrix theory [BGS84].

An effect where we observe the chaotic nature of a system in contrast to an integrable one is given by thermalization. In quantum mechanics there are various approaches to this topic [Deu91; RS12]. The basic question is, how a system which is initialised in a (highly) excited state evolves in time. How does the corresponding time evolution of an observable looks like?

We consider an initial excited state which has evolved in time

$$|\psi(t)\rangle = \sum_{\alpha} c_\alpha e^{-iE_\alpha t} |\alpha\rangle \tag{2.1}$$

where $|\alpha\rangle$ denote a basis of the Hamiltonian with eigenenergy E_α and c_α are the corresponding coefficients at initial time $t = 0$. Then the expectation value of an observable with this state can be written as

$$\langle \mathcal{O} \rangle_t = \langle \psi(t)| \mathcal{O} |\psi(t)\rangle = \sum_{\alpha,\beta} c_\alpha c_\beta^* e^{-i(E_\alpha - E_\beta)t} \langle \beta| \mathcal{O} |\alpha\rangle \tag{2.2}$$

which is dependent on the initial coefficients c_α's, the energy differences and the matrix element of $\mathcal{O}$. The eigenstate thermalization hypothesis (ETH) [Sre94; Sre99] states that the condition of thermalization is that this expectation value converges to the expected value of a microcanonical ensemble of a subsystem independent of the initial state

$$\overline{\langle \mathcal{O} \rangle}_t \approx \langle \mathcal{O} \rangle_{micro} \tag{2.3}$$

where $\overline{\langle \mathcal{O} \rangle}_t$ denotes the long-time average and $\langle \mathcal{O} \rangle_{micro}$ the average for a microcanonical ensemble [RS12]. An intuition for this is given in considering that a part of the ensemble acts as a bath for the smaller ensemble [NH15].

In general, it is believed that chaotic models fulfil the ETH and tend to thermalize while integrable models do not [Sre94; RS12]. However, the overall connection is still highly discussed [RDO08; Rig09; NH15; Aba+19]. Still, we gain an idea of what the more likely outcome is going to be.

Coming back to equation (2.2), we find that the dynamics of a system are influenced by the exponential function containing the energy difference. For instance, a part of the thermalization process is the reduction of the sum to only its diagonal part $\alpha = \beta$. This is achieved by a dephasing of the non-diagonal terms over long times and requires non-degenerate energies [Sre99]. Such spectral properties differ for integrable and chaotic systems, as the expectation on the level spacings is different. While we find the level clustering for integrable systems [BT77], chaotic systems exhibit level repulsion [Meh04].

2.2 Level Statistics

After our short introduction to thermalization in quantum systems we now want to find a way to determine whether a system is integrable or not. Identifying a chaotic

quantum system has to be approached differently than in classical mechanics. An effective method is using the spectrum by considering the properties of level statistic.

The idea of an analysis of the level statistics is to break the spectrum down to all simultaneously present symmetries for a chaotic system and check its statistical nature. Therefore, the foundation is given by the ordered spectrum of a model respecting all of its symmetries. These symmetries need to commute so that we can find a common eigenbasis. With this ordered spectrum $\{E_1, E_2, \ldots, E_M\}$ we can calculate the consecutive level spacing

$$\delta_j = E_{j+1} - E_j.$$

Now let us discuss what to expect for the two cases of integrability and chaos. For chaotic models we have already discussed its approximation by random matrix theory. Depending whether the system respects time reversal symmetry or not, we can expect the behaviour given by a Gaussian Orthogonal Ensemble (GOE), Gaussian Unitary Ensemble (GUE) or the Gaussian Symplectic Ensemble (GSE). In our case, we only consider the GOE case as all models are time reversal symmetric. In random matrix theory the distribution of level spacings $P(\delta/\Delta)$ can be approximated by the Wigner surmise

$$P_{\mathrm{GOE}}(\delta/\Delta) = \frac{\pi}{2}\frac{\delta}{\Delta}\exp\left(-\frac{\pi}{4}\frac{\delta^2}{\Delta^2}\right) \tag{2.4}$$

as elaborated in [Meh04].

In the integrable case it is argued that the level spacing represents a Poisson distribution. A more detailed derivation of this statement can be found in [BT77]. The Poisson distribution then takes the form

$$P_{\mathrm{Poisson}}(\delta/\Delta) = \exp\left(-\frac{\delta}{\Delta}\right). \tag{2.5}$$

These distributions are depicted in figure 1.

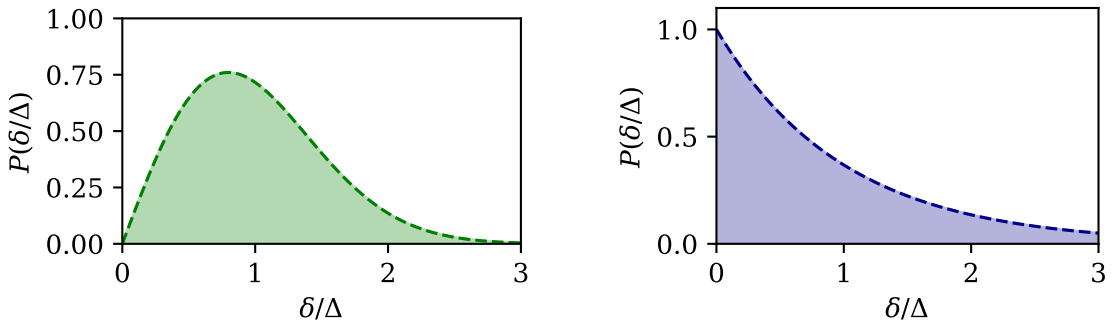

(a) GOE distribution

(b) Poisson distribution

Figure 1: Expected distributions of the consecutive level spacings δ for the Poisson and GOE case.

With these distributions we already observe the difference between the level spacings discussed in section 2.1. The level repulsion for chaotic models can be seen in

the distribution of δ in the GOE case in equation (2.4) as it vanishes for small level spacings $\delta = 0$. However, the Poisson distribution reaches its maximum at this point supporting level clustering.

An important part of the distributions above is the mean spacing Δ. Analysing the level spacing requires unfolding the spectrum which is not trivial to perform and an imprecise conduction may influence the result [Góm+02]. In general, an approach is to extract the local density of states [GMW98]. A way to circumvent this problem is to use the ratios

$$r_j = \frac{\min(\delta_j, \delta_{j+1})}{\max(\delta_j, \delta_{j+1})} \tag{2.6}$$

of two consecutive level spacings [OH07].

In the GOE case the corresponding distribution $P(r)$ was derived [Ata+13]

$$P_{\text{GOE}}(r) = \frac{27}{4} \frac{r + r^2}{(1 + r + r^2)^{5/2}} \tag{2.7}$$

while for the Poisson distribution we obtain [OH07]

$$P_{\text{Poisson}}(r) = \frac{2}{(1 + r)^2}. \tag{2.8}$$

Therefore, we lose the problematic Δ dependence. Moreover, the ratios r are only in the interval $[0, 1]$ which simplifies displaying the statistics. These two distributions are depicted in figure 2.

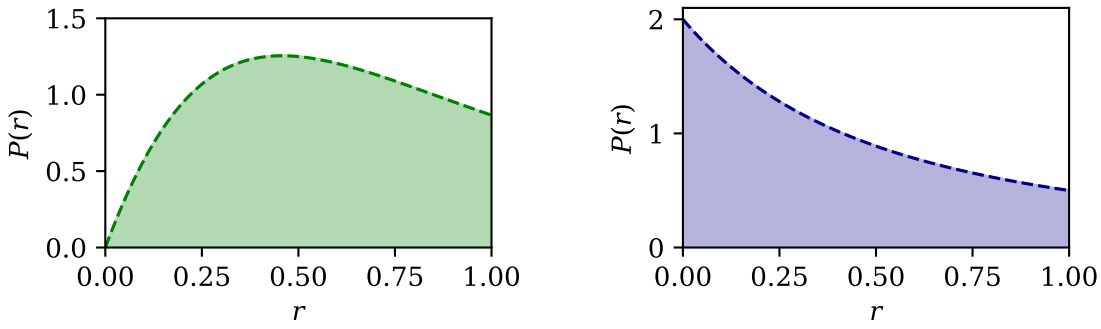

(a) GOE distribution

(b) Poisson distribution

Figure 2: Expected distributions of the ratios of consecutive level spacings r for the Poisson and GOE case.

It may be overwhelming to consider level statistics for many parameters by plotting them individually. An often used quantity for this is the mean ratio $\langle r \rangle$ defined by

$$\langle r \rangle = \int_0^1 P(r) r dr = \sum_{i=0}^{n} P(r_i) r_i \Delta r \tag{2.9}$$

where the second part covers the discrete case with n intervals of width Δr. The values for the different distributions are [Ata+13]

$$\langle r \rangle_{\mathrm{GOE}} = 0.536 \quad \text{and} \quad \langle r \rangle_{\mathrm{Poisson}} = 0.386. \tag{2.10}$$

With this tool at hand, it seems simple to determine whether a system is chaotic or not. We only need to generate the spectrum, calculate the ratios and check which distribution fits best to a histogram of these ratios. However, one problem remains. We only find P_{GOE} if all symmetries are considered. Otherwise, the distribution of ratios is going to be an overlap of various GOE sectors. The exact shape of this function can be calculated numerically [Gir+22] and is dependent on the number of symmetries missing and the size of the respective sectors. If only very few symmetries are missing it is a useful tool to find the remaining ones. Yet, the more symmetries are not respected the more the distribution merges into a Poisson distribution.

The consequence is clearly problematic. A Poisson distribution is never a reliable single indicator of an integrable model. It might still be that missing symmetries prevent us from seeing its actual shape. In contrast, finding a GOE distribution is an indicator for a chaotic model as it cannot be obtained by superposing Poisson distributions.

2.3 Extensions of the Fermi-Hubbard Model

The Fermi-Hubbard model is a basic yet versatile model. We consider a one dimensional chain of length L where each site can be seen as a minimum of a periodic potential. We consider N fermions located at the different sites of the chain. Due to the Pauli exclusion principle, each site can at most be filled with two fermions having opposite spin. The Fermi-Hubbard Hamiltonian takes the form

$$H_{\mathrm{FH}} = -t \sum_{\sigma \in \{\uparrow,\downarrow\}} \sum_{j=1}^{L} \left(c_{j\sigma}^{\dagger} c_{j+1\sigma} + c_{j+1\sigma}^{\dagger} c_{j\sigma} \right) + U \sum_{j=1}^{L} n_{j\uparrow} n_{j\downarrow} \tag{2.11}$$

where $c_{j\sigma}^{\dagger}$ ($c_{j\sigma}$) is the creation (annihilation) operator of spin σ acting on site j and $n_{j\sigma}$ is the number operator. Moreover, t denotes the hopping amplitude and U the interaction strength. We impose periodic boundary conditions. The action of the Hamiltonian is depicted in figure 3. The first term of the Hamiltonian corresponds to a hopping of a particle between two neighbouring sites with the hopping amplitude t, whilst the second part describes an interaction between two particles of opposite spin located on the same site. On the basis of the Bethe Ansatz, Lieb and Wu [LW68] found an analytic solution which makes the Fermi Hubbard model integrable.

There are two extensions to this model that are of interest for this thesis. Firstly, we can introduce a potential varying over every other site. Thus, the new Hamiltonian is given by

$$H_{\mathrm{Ion}} = H_{\mathrm{FH}} - \mu \sum_{\sigma \in \{\uparrow,\downarrow\}} \sum_{j=1}^{L} (-1)^j n_{j\sigma} \tag{2.12}$$

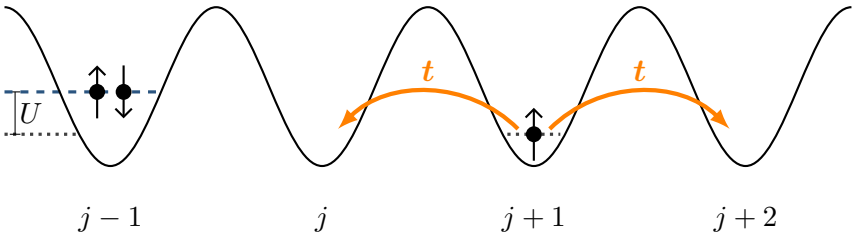

Figure 3: Visualization of the Fermi Hubbard model. The sites are located at the potential minima. Particles can hop on a neighbouring site by tunnelling the potential with amplitude t. Two particles with opposite on the same site interact resulting in a raise by U. Note that the Pauli exclusion principle holds.

with μ denoting the potential. It is depicted in figure 4a. The potential minima are shifted for even sites by $-\mu$ and for odd sites by $+\mu$ resulting in a difference of 2μ between neighbouring minima. In literature, this is usually referred to as the ionic Hubbard model. The analysis done in this thesis has already been conducted for this model in [De +22]. For the sake of comparison, we are going to refer back to this model and its analysis.

For the second extension, we vary the hopping amplitudes. Instead of having a site-independent hopping amplitude t, we obtain alternating hopping amplitudes t and t' changing every other site. The corresponding Hamiltonian is given by

$$H_{\text{Dim}} = -t \sum_{\sigma\in\{\uparrow,\downarrow\}} \sum_{\substack{j=1 \\ \text{odd}}}^{L} c^\dagger_{j\sigma} c_{j+1\sigma} - t' \sum_{\sigma\in\{\uparrow,\downarrow\}} \sum_{\substack{j=1 \\ \text{even}}}^{L} c^\dagger_{j\sigma} c_{j+1\sigma} + \text{h.c.} + U \sum_{j=1}^{L} n_{j\uparrow} n_{j\downarrow} \tag{2.13}$$

and is also depicted in figure 4b. This model is called the dimerized Hubbard model. Note that, in contrast to the Fermi Hubbard model, both extensions display a bipartite lattice structure. As we impose periodic boundary conditions, only an even number of sites is possible.

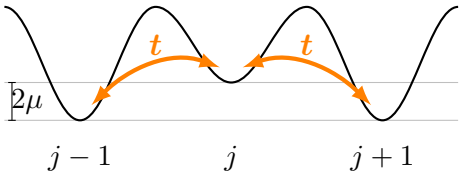

(a) Ionic Hubbard Model

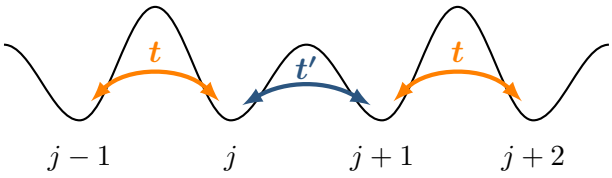

(b) Dimerized Hubbard Model

Figure 4: Visualization of the two considered extensions of the Fermi Hubbard model. On the left hand side we find the ionic Hubbard model. An additional potential term results in a difference between neighbouring minima of 2μ. On the right hand side the dimerized Hubbard model is depicted. Alternating potential walls result in alternating hopping amplitudes t and t' over every other site.

2.3.1 Symmetries

We have seen in section 2.2 that symmetries play a crucial role for analysing the level statistics. Therefore, it will be of great importance to know and understand all of the underlying symmetries of a model. As the Fermi Hubbard model is integrable, an analysis of its symmetries can be very extensive. Yet, some basic symmetries can be translated to symmetries also present in the extensions of the Hubbard model which are of interest for us. Nevertheless, we are not going into detail about the symmetries of the Hubbard model and restrict ourselves to a discussion of the symmetries for the extensions. Many of those were already discussed in [De +22].

Translation Symmetry In the Hubbard model a translational symmetry is present. It takes the form

$$T c_{j\sigma} T^\dagger = c_{j+1\sigma} \tag{2.14}$$

which can be understood as all particles being shifted by one site. In both extensions, this symmetry is broken by either the potential or the alternating hopping amplitudes resulting in the mentioned bipartite lattice structure. Nevertheless, we can still find an analogue given by a two-site translational invariance

$$T_2 c_{j\sigma} T_2^\dagger = T^2 c_{j\sigma} (T^2)^\dagger = c_{j+2\sigma}. \tag{2.15}$$

The conserved quantity for this symmetry is the momentum $k' = 4\pi k/L$ originating from the eigenvalues $e^{ik'}$ of the translation operator T_2 where $k \in \{0, 1, \dots L/2-1\}$ is integer. Note that the factor of 4 in the momentum arises as we consider a translation by two sites. We will often use the integers k for the momenta k' to shorten notation.

Reflection Symmetry Another symmetry originating from the basic Hubbard model is the reflection symmetry

$$R_b c_{j\sigma} R_b^\dagger = c_{L+1-j\sigma}. \tag{2.16}$$

Here, the index of R denotes the type of reflection, in this case reflection at a bond. Similarly, it is also possible to define the reflection at a site R_s

$$R_s c_{j\sigma} R_s^\dagger = c_{L-j\sigma} \tag{2.17}$$

which yields the same result up to notation. Furthermore, it is independent of the choice at which site or bond the model is reflected due to the translation symmetry.

It is important to note that translation and reflection symmetry in general do not commute. Only the momenta $k' = 0$ and $k' = \pi$ hold an exception to this rule.

For both extensions of the Fermi Hubbard model a reflection symmetry is present. However, the exact definition of the reflection depends on the respective model. As we can see in figure 4, the ionic Hubbard model is symmetric around a site due to the different on-site potentials. In contrast the alternating hopping amplitude results in a reflection symmetry at the bond. The two models with the different types of

reflections are displayed in figure 5. Therefore, it is important to consider the correct type of reflection while analysing the individual models. As for the Hubbard model, the reflection symmetry only commutes with the translation symmetry for $k' = 0$ and $k' = \pi$.

(a) Dimerized structure (b) Ionic structure

Figure 5: Visualization of the two different reflections R_b and R_s. Dots represent sites while lines represent bonds. Different coloured bonds correspond to different hopping amplitudes and different coloured sites to different on-site potentials. We can observe that in order to stay invariant after reflection both model types requires different types of reflection.

Spin Rotation Symmetry One of the basic symmetries of the Hubbard model is the $SU(2)$ spin rotation symmetry. The components of the spin operator are defined by

$$S_\alpha = \frac{1}{2}\sum_{j=1}^{L}\sum_{a,b\in\uparrow,\downarrow} c_{ja}^\dagger(\sigma^\alpha)_{ab}c_{jb} \tag{2.18}$$

where σ^α denote the corresponding Pauli matrices. All three operators S_α commute with the Fermi Hubbard model as well as its extensions. However, we find that only two operators commute with each other as it is well known from quantum mechanics. Therefore, we keep the convention of using the total spin S^2 and the S_z component leading to the well known conservation of the total spin s for S^2 and the spin z-component m for S_z.

Pseudospin η-Pair Symmetry It is possible to construct an SU(2) symmetry similar to the spin symmetry using the definitions

$$\eta_+ = \sum_{j=1}^{L}(-1)^{j+1}c_{j\uparrow}^\dagger c_{j\downarrow}^\dagger, \qquad \eta_- = \eta_+^\dagger = \sum_{j=1}^{L}(-1)^{j+1}c_{j\downarrow}c_{j\uparrow}$$
$$\text{and} \quad \eta_z = \frac{1}{2}(N-L).$$

The ladder operators $\eta_\pm$ create or annihilate a superposition of states with a spin up and spin down particle on the same site. Consequently, it can be interpreted as creating a pair state.

The defined operators satisfy the commutation relation of the SU(2) algebra and, furthermore, we can define

$$\eta^2 = \frac{1}{2}(\eta_+\eta_- + \eta_-\eta_+) + (\eta_z)^2.$$

Similar to the spin symmetry, η_z and η^2 commute with the Hamiltonian. This is not surprising for the η_z as it is linear in the conserved particle number N. In contrast, the η^2 yields a new conserved quantity ξ. For η_z we denote the conserved quantity with $\tilde{n}$.

A notable difference from the spin rotational symmetry is the commutator of the ladder operators and the Hamiltonian. In the spin symmetry the two operators commute, whereas the η-pair ladder operators obey

$$[H, \eta_\pm] = \pm U \eta_\pm. \tag{2.19}$$

This fits our notion of $\eta_\pm$ creating or annihilating pairs as this results in a breaking of the invariance in the interaction term H_U. Based on this commutator's properties, this algebra is called a Spectrum Generating Algebra. For more details we refer to the Appendix B and [MRB20; Ess+05].

The η-pair symmetry is present for the Hubbard model as well as the dimerized Hubbard model. In contrast, the potential of the ionic Hubbard model in equation (2.12) breaks this SU(2) symmetry.

Gauge Symmetry In all discussed models, we can apply a $U(1)$ gauge transformation to the creation and annihilation operator

$$G c_{j\sigma} G^\dagger = e^{i\phi} c_{j\sigma} \tag{2.20}$$

for which the Hamiltonians are invariant. This symmetry results in the conservation of the particle number N_σ in the respective spin sector. Hence, the total particle number $N = N_\uparrow + N_\downarrow$ is also conserved. These conservation laws are already included by the spin z- component $S_z = \frac{1}{2}(N_\uparrow - N_\downarrow)$ and the $\eta_z = \frac{1}{2}(N - L)$.

Particle-Hole Symmetry A particle-hole symmetry describes the invariance when interchanging particles and holes, where the holes correspond to the absence of a particle. One of the major findings when analysing the ionic Hubbard model ([De +22]) was the existence of a particle-hole like symmetry

$$F_{\text{ion}} c_{j\sigma} F_{\text{ion}}^\dagger = (-1)^j c_{j+1\sigma}^\dagger \tag{2.21}$$

for half filling where we define the filling as the number of particles per twice the number of sites $n = N/(2L)$. This symmetry cannot be present for other fillings, as the same number of holes and particles with both spins is necessary. For the dimerized Hubbard model with alternating hopping we can also find such a particle hole symmetry

$$F c_{j\sigma} F^\dagger = (-1)^j c_{j\bar{\sigma}}^\dagger \tag{2.22}$$

with $\sigma \neq \bar{\sigma}$. As for the ionic model, it is only present for half filling. However, this symmetry is already included in the η-pair symmetry as discussed in Appendix B.

Simultaneously present symmetries Not all of the introduced symmetries are simultaneously present for both extensions of the Hubbard model. For the ionic Hubbard model as summarized in [De +22], we can divide the system into subsectors with the corresponding conserved quantities N, k, s, m. Additionally, for $k' = 0$ or $k' = \pi$ we find the parity subsectors p and, furthermore, for half filling with $N = L$ the charge conjugation subsectors.

For the dimerized Hubbard model we also have the N, k, s, m subsectors with the parity p for $k' = 0, \pi$. Furthermore, the η-pair symmetry yields the ξ subsectors. Again, note that we can either use the number of particles N as a conserved quantity or, equivalently, the η_z component $\tilde{n}$. The more unified set of quantities would be $k, (p), s, m, \xi, \tilde{n}$. However, the particle number is regarded as more intuitive. As a consequence, in this thesis we are going to use the set $N, k, (p), s, m, \xi$. This sums up all commuting symmetries of the dimerized Hubbard model that are known to us at this point.

3 Implementation of the Symmetries

In order to analyse the properties of the level statistics of a model, the first task is to generate the energy spectrum divided into its symmetry subsectors. In general the energies are obtained by diagonalising the Hamiltonian. In our case it is important to determine all the energies as accurately as possible. Therefore, the variety of efficient algorithms is limited, since most of these focus only on calculating certain areas of the spectrum, e.g. groundstate energies. Moreover, the size of the Hamiltonian and, hence, the computational cost for the diagonalization highly increases with system size. In summary, this results in severe limitations of system sizes we can consider.

Fortunately, it is not necessary to calculate the whole spectrum at once. The symmetries discussed before induce a block diagonal structure for the Hamiltonian if the correct basis is chosen. This can be used to break the Hamiltonian down into smaller blocks which then can be diagonalised. In the following, we are going to discuss this procedure and its implementation for some of the symmetries. For the exact diagonalization we use the ideas and derivations from [WF08; San10]. Afterwards we discuss the implementation of the remaining symmetries where we utilize other techniques.

3.1 Exact Diagonalization

Let us consider a Hamiltonian matrix H, which we want to diagonalise to obtain the energy eigenvalues. As a basis we choose the states

$$|s\rangle = |n_{1\uparrow} n_{2\uparrow} \dots n_{L\uparrow} | n_{1\downarrow} n_{2\downarrow} \dots n_{L\downarrow}\rangle = \prod_{i\in I} c^\dagger_{i\uparrow} \prod_{j\in J} c^\dagger_{j\downarrow} |0\rangle \tag{3.1}$$

with $n_{i\sigma} \in \{0, 1\}$ and I and J being the sets containing the sites where spin up or respectively spin down particles are located. Note that the ordering is chosen such that the operators with the last sites act first. Without any restrictions, the number of basis states for a given length L would be 2^{2L}. Thus, even for considerably small system sizes the complete Hamiltonian matrix becomes large. Moreover, only a minor increase in the length L will yield a significant increase in the matrix dimension. Therefore, we are only able to diagonalise rather small system sizes, i.e. $L = 8$, on an average computer.

However, the symmetries of the Hamiltonian yield a useful feature. Consider a symmetry operator S corresponding to a symmetry of H. By definition the symmetry operator commutes with the Hamiltonian, $[H, S] = 0$. Now let us assume we find an eigenbasis of S. Applying the Hamiltonian H to an eigenvector of S cannot change its eigenvalue regarding S as they commute. This induces a block diagonal structure for H where each block corresponds to one eigenvalue of S. This can be generalised for more symmetries S_i if they commute with each other, $[S_i, S_j] = 0$. A visualization of a matrix before and after considering the symmetries is shown in figure 6.

This yields many benefits. We can now diagonalize the blocks of the Hamiltonian individually, which saves great computational cost. Furthermore, diagonalizing the whole Hamiltonian would have required to assign the eigenenergies in the respective

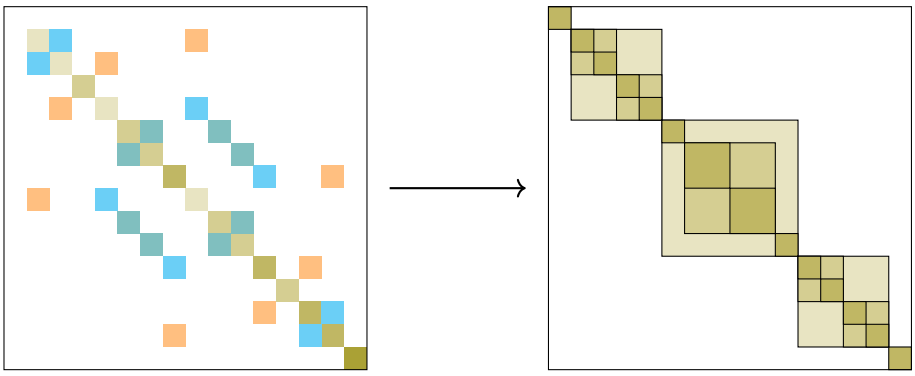

Figure 6: Non-zero matrix elements of the dimerized Hubbard Hamiltonian for $L = 2$ in position basis (left hand) and in symmetrized basis (right hand). Different colours in the left matrix represent different entries. Different colour gradients in the right matrix represent the amount of symmetries considered. We observe how in the symmetrized basis the block diagonal structure is formed. Adapted from [WF08].

symmetry sectors afterwards. By doing an exact diagonalization, the symmetry subsectors are formed naturally. With this methodology, we are now able to compute significantly larger systems by breaking down the matrix into blocks while also gaining the correct assignments of the eigenvalues. Nevertheless, an obvious drawback is that we first have to construct the simultaneous eigenbasis of the symmetry operators.

This seems simple at first whilst looking at the particle number and spin S_z conservation. For both, our initial choice of basis is already an eigenbasis. Yet, considering the spatial symmetries, namely the translation and reflection symmetry, becomes more involved as we have to construct a fairly complicated eigenbasis for both symmetries simultaneously. Nevertheless, the most complex basic symmetries turn out to be the total spin symmetry S^2 and the total pseudo spin η^2, as it is complicated to find their eigenbasis. In general the more symmetries one simultaneously implements, the more challenging the construction becomes. Therefore, we are only going to implement the number and spin S_z conservation as well as the two spatial symmetries for our exact diagonalization routine. The two remaining symmetries, S^2 and η^2, are considered after the exact diagonalization.

3.2 Implementation of the Exact Diagonalization

Even though the idea of constructing an eigenbasis is straightforward while doing it by hand, it is another matter implementing it for general parameters. Before we consider the implementation of the symmetries, the first task is to find a way to denote the states in an efficient way. For this purpose, recall the representation of a state introduced in equation (3.1). Each state has a unique label, namely the particle number on each site for each spin. Here, we follow the convention of first writing the spin up section of the chain before writing the spin down section as this notation has some advantages over the course of the implementation.

The key point of this labelling is that fermions only allow values $n_{i\sigma} \in \{0, 1\}$.

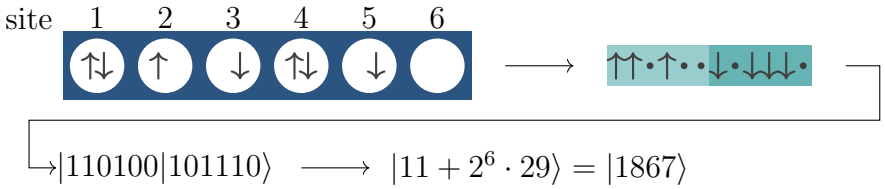

Figure 7: Example on how to transform a state in position basis to an integer. We first divide the particles into spin chains. Moreover, particles are denoted by 'ones' and holes by 'zeros'. With the received bit number we are able to calculate an integer.

Hence, we obtain a sequence corresponding to a $2L$ bit long integer. With our notation we can write

$$M = M_\uparrow + 2^L M_\downarrow$$

where M_σ denotes the integer corresponding to each spin chain and M denotes the integer number corresponding to the complete state. Here, against convention we read the bit number from left to right. An example is shown in figure 7.

As a consequence, we can now identify each state in the position basis with an integer. For a fixed system size L with N particles this corresponds to all integers from 0 to $4^L - 1$. Still, the positions of the particles for both spins are simple to extract by displaying the integer as a bit number. Moreover, the operations on bit numbers are a helpful tool for many symmetries. Therefore, it is only necessary to save the integer and extract all of the information if needed.

3.2.1 Particle Number and Spin S_z Conservation

As discussed previously, the particle Number N and spin S_z conservation are the easiest to implement. We only need to find all the states containing the correct particle number and spin. Therefore, the best approach is to construct the states iteratively.

Let us first consider the particle number. In the $2L$ bit number representation having a certain number of particles corresponds to having the same number of '1's. Hence, we have to construct all the states containing N times '1'. This can be done recursively in a way that already memorizes the states in order.

For the spin conservation most of the work is already done. Knowing the number of particles and the total spin S_z, it is straightforward to find the number of spin up and spin down particles of the states

$$N_\uparrow = \frac{N}{2} + S_z, \quad N_\downarrow = N - N_\uparrow = \frac{N}{2} - S_z.$$

Hence, we can use the function of the number conservation symmetry to find the states having N_σ particles for an L long bit number. After combining all states for the spin up and spin down section with each other we obtain an ordered list of all states for a given N and S_z.

3.2.2 Spatial Symmetries and Representatives

The problem of the spatial symmetries is that applying the symmetry operators T_2 and R to a state most likely yields a different state. Therefore, the new basis contains superpositions of up to $L/2$ states. Hence the question of how to memorize these states arises.

At first glance an unintuitive yet very practical way is to save a representative for each such state [WF08]. In our case, we define this representative as the state with the lowest bit number. Hence, for each superposition of states we only memorize one state and it contains a great part of the relevant information for the construction.

Let us further elaborate the advantages of this method. Consider a projection operator of a symmetry P that projects onto its symmetry subsectors. A normalized eigenstate of the symmetry takes the form

$$|\tilde{s}\rangle = \frac{P\,|s\rangle}{\sqrt{\langle s|\,P\,|s\rangle}} = \mathcal{N} P\,|s\rangle$$

where $\mathcal{N}$ corresponds to the normalization constant. Furthermore, consider an entry of the Hamiltonian matrix

$$\langle \tilde{s}_1|\,\hat{H}\,|\tilde{s}_2\rangle = \langle s_1|\,P\hat{H}P\,|s_2\rangle\,\mathcal{N}_1\mathcal{N}_2.$$

We can observe that computing this matrix element becomes tedious as we have to apply the Hamiltonian to all the states in the eigenstate $|\tilde{s}_2\rangle$ and afterwards calculate the scalar product with $\langle \tilde{s}_1|$. A way to circumvent this problem is given by the following simple calculation

$$\begin{aligned}\langle \tilde{s}_1|\,\hat{H}\,|\tilde{s}_2\rangle &= \langle s_1|\,P\hat{H}P\,|s_2\rangle\,\mathcal{N}_1\mathcal{N}_2\\ &= \langle s_1|\,P^2\hat{H}\,|s_2\rangle\,\mathcal{N}_1\mathcal{N}_2\\ &= \langle s_1|\,P\hat{H}\,|s_2\rangle\,\mathcal{N}_1\mathcal{N}_2.\end{aligned}$$

Here, we have used that $[H, P] = 0$ as P by definition only contains powers of the symmetry operator that commute with H. It is still necessary to consider the scalar product with $\langle \tilde{s}_1|$ in the end. Yet, we only need to apply the Hamiltonian to the representative state and still obtain the correct matrix entry which is a noticeable simplification from the procedure above.

Explicitly, the following steps are conducted. First, we consider all states available at this point and check which representative can be assigned to them. Furthermore, we need to keep track of the corresponding coefficient relative to the representative in some sort, e.g. saving it in a dictionary, in order to access it later. Another advantage we encounter at this point is that the number of representatives is also the size of the block of the Hamiltonian. To compute the matrix entries, we now apply the Hamiltonian to the different representatives and deduce from our saved coefficients the correct factors given by the final scalar product.

The procedure does not change significantly for more than one symmetry. In this case we have to consider two projection operators instead of one. Still, we only need to apply the Hamiltonian to the representatives and check the coefficients afterwards, since both projection operators commute due to the commutation of the symmetry operators.

Now, that we have simplified the construction of the Hamiltonian matrix successfully, we still have to consider one major difficulty. The correct calculation of the coefficients combined with the assignment to the appropriate eigenvalues is very intricate. As we consider fermions, the creation and annihilation operators anticommute. Thus, signs have to be checked very thoroughly and tend to have a disarranging influence on the eigenstate construction. We are going to elaborate this in the following sections and with more details in Appendix C.

Translation symmetry The projection operator for the translation symmetry takes the form

$$P_t(k) = \frac{2}{L} \sum_{l=1}^{L/2} e^{ilk} T_2^l$$

where T_2 is the two-site translation and k denotes the momentum. Applying this projection operator to a state $|s\rangle$ yields an unnormalised eigenstate of T_2 containing all possible translations of $|s\rangle$. We shall set aside the task of finding the correct normalization for now and, quickly, discuss the influence of the fermionic anticommutations.

At first glance, applying the translation operator T_2 to a state seems simple. Each spin chain has to be shifted by two sites

$$|n_{1\uparrow} \dots n_{L\uparrow}|n_{1\downarrow} \dots n_{L\downarrow}\rangle \longrightarrow |n_{L-1\uparrow} n_{L\uparrow} n_{1\uparrow} \dots n_{L-2\uparrow}|n_{L-1\downarrow} n_{L\downarrow} n_{1\downarrow} \dots n_{L-2\downarrow}\rangle \,.$$

Implementing such a shift does not require much effort as the chains can always easily be separated by the 2^L prefactor of the spin down chain. Furthermore, a bit shift is either way already implemented the used programming language or can be written by using common bit number knowledge.

Yet, by translating the state an additional sign might emerge. We find the origin of this sign in our chosen representation in equation (3.1) considering the creation operators. After projecting the creation operators to their translated picture the given order is disturbed. To stay consistent, we need to commute the creation operators to their correct order. In general, we can find that for a single site translation the commutation yields an additional sign if, firstly, a single particle is shifted from the last two sites to the first two sites and, secondly, the number of particles in the spin sector N_σ is even (see Appendix C).

As we consider the two site translation T_2, in the cases of odd particle numbers in the spin sectors N_σ or two particles shifting in one step no change of sign can occur. For all the other cases we have to save the sign as it is part of the prefactor in the eigenstate. Moreover, the sign can cause other complications further explained below.

It might happen, that the original state $|s\rangle$ is obtained after less than $L/2$ translations. A quite basic example is a state where every second site is occupied. In this

case we only need a single two site translation to obtain the original state. First of all, this complicates the normalization. In general the translation operator yields a sum of $L/2$ states which does not exclude the case of all translations being the same. For determining the normalization constant, however, it is vital to know how many unique states can be found in an eigenstate.

Furthermore, it might happen that due to arising signs a state completely cancels. A simple example for such a state is given by

$$T_2 \, |0101 \ldots 0101|000 \ldots 0000\rangle = - \, |0101 \ldots 0101|000 \ldots 0000\rangle$$

for $N_\uparrow$ even. Applying $P_t(k = 0)$ will cancel this state while applying $P_t(k = L/4)$ (if possible) would not, even though in the first place we would expect the opposite.

This discussion just scratches the surface of the addressed difficulties as we have only gained a basic understanding of the exceptional cases. Yet for the implementation it is necessary to find universal procedures for constructing and assigning the eigenstates. We are not going into further detail of the technicalities and solutions that can be found. A more detailed, yet not complete discussion can be found in Appendix C. But in conclusion, we can emphasize that all signs need to be handled with care.

Reflection symmetry For the reflection symmetry we can continue in a similar manner. The projection operator is given by

$$P_r(p) = \frac{1}{2}(1 + pR)$$

where $p = \pm 1$ denotes the parity. For the reflection operator R we can choose an arbitrary bond to reflect at because of the translation symmetry. Hence, in our case the chain is reflected in the middle

$$|n_{1\uparrow} \ldots n_{L\uparrow}|n_{1\downarrow} \ldots n_{L\downarrow}\rangle \longrightarrow |n_{L\uparrow} n_{L-1\uparrow} \ldots n_{2\uparrow} n_{1\uparrow}|n_{L\downarrow} n_{L-1\downarrow} \ldots n_{2\downarrow} n_{1\downarrow}\rangle \, .$$

Again the anticommuting of the creation operators may result in an additional sign. Indeed, one can find that if $(N_\sigma^2 - N_\sigma)/2$ is odd, a minus sign arises (see Appendix C). Moreover, as for the translation symmetry, a state can be reflected on itself. Once more this requires us to be careful when determining the normalization constants and the correct assignment to the eigenvalues because some states will in fact cancel themselves. Still, as the reflection only connects at most two states to a new eigenstate the construction turns out to be slightly simpler.

A final challenge is connecting both reflection and translation symmetry. As discussed before, the two projection operators only commute for $k = 0$ or $k = L/4$ where the latter momentum is not always possible as L is not necessarily a multiple of 4. The general procedure is similar to before with the only difference being that we have to find the representatives and coefficients for both symmetries simultaneously. In the end, combining these symmetries requires caution and a good overview of all coefficients.

3.3 Testing Methods

Due to the many signs and different coefficients, the assignments of the states to the correct symmetry eigenvalues is error-prone. Therefore, the exact diagonalization routine requires thorough testing. Such testing methods vary from checking the hermitian shape of the Hamiltonian to comparison against analytic results. In the end, it is important to consider a wide range of tests to make sure the written diagonalization works as intended as it is the back bone of the following analysis. Moreover, this also provides us with estimates on the accuracy of the implementation.

Imaginary Parts and Spin Degeneracy An initial simple way of testing if the general structure of the Hamiltonians is correct is checking the imaginary parts of the eigenvalues. As H is hermitian, all the eigenvalues should be real. Therefore, we can easily check this by testing if all imaginary parts are zero. Moreover, for the spin S_z quantum number the eigenvalues in the $\pm m$ sectors are degenerate. By comparing the eigenvalues in those respective sectors, it is possible to verify this degeneracy.

Full Hamiltonian Comparison Up to certain system sizes it is possible to diagonalize the complete Hamiltonian for a given L, N and S_z. By comparing the eigenvalues of the whole Hamiltonian to the ones we obtain by the spatial symmetry blocks we can assure whether the norms, signs and, thus, the coefficients are calculated correctly. Major errors should become apparent here.

Non-Interacting Regime Comparison Setting $U = 0$ the model becomes analytically solvable. The solution is given in the appendix A. In this regime, we may compare the generated eigenvalues in the translation sectors to the analytic results. Unfortunately, this does not yield us any information whether the assignment to the reflection sectors has worked.

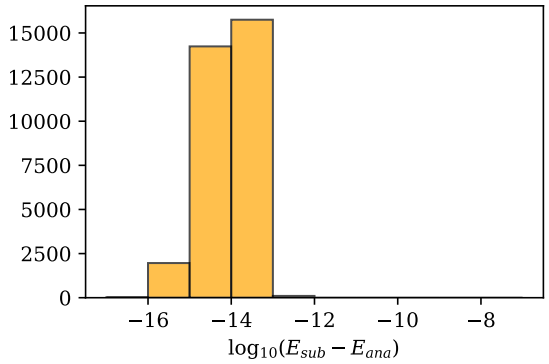

Figure 8: Differences between analytic results and numerical results for $t'/t = 2$, $U/t = 0$, $L = 12$, $N = 6$, $m = 0$ for all k sectors combined. The x-axis is decadic logarithmic. We verify the results and note that the deviations are of order 10^{-12}.

For the last method, the comparison to the analytical solution, an exemplary histogram is shown in figure 8. The differences between the analytics results and the eigenvalues obtained by the exact diagonalization are displayed in a histogram. The decadic logarithmic axis shows the order of deviation. We observe that the differences are at least of order 10^{-12} and, thus, the numerical results fit the analytic expectations very well.

3.4 Implementation of the Remaining Symmetries

To obtain the correct distribution for the level statistics it is necessary to assign the eigenvalues to all symmetry sectors. After the exact diagonalization we obtain the energies in N, k, p, m subsectors and we still need to implement the two remaining symmetries, namely the spin S^2 and η^2 symmetry.

For the spin S^2 symmetry there exists a simple procedure to find the symmetry sectors which is introduced in e.g. [Poi+93] or [De +22] using the commutation relations of the ladder operators. In contrast, the η-pair symmetry is not so prominent but exhibits a very similar structure. We find that we can utilize the same approach with small adjustments.

3.4.1 Spin S^2 Symmetry

The procedure used for the spin symmetry takes advantage of the commutator $[H, S_\pm] = 0$. Now consider a state $|s, m\rangle$ with an energy $E_{s,m}$. Acting with $S_\pm$ on this state increases or respectively decreases m while s is invariant. As we know that the ladder operator commutes with the Hamiltonian this new state $|s, m \pm 1\rangle$ has the same energy $E_{s,m} = E_{s,m\pm1}$.

This can be utilized by starting with the state identified with $m_{\max}$ given by $|s, m_{\max}\rangle$. Recall that the spin z-component m can only take the values $-s, -s+1, \ldots, s-1, s$. Therefore, for maximal m the only valid total spin s is again the z-component $|s, m_{\max}\rangle = |s = m_{\max}, m_{\max}\rangle$. As a consequence, all eigenvalues assigned to the $m = m_{\max}$ are already known to be the only energies in the $s = m_{\max}$ sectors.

Furthermore, a state with $m = m_{\max} - 1$ can either have total spin $s = m_{\max}$ or $s = m_{\max} - 1$. However, we already know that because of the ladder operators a state of the $s = m_{\max}$ sectors has the same eigenenergy as one of the states in the $m = m_{\max}$ sector. Therefore, when considering the energies of the $m = m_{\max} - 1$ sector it is only necessary to identify all eigenvalues from the $m = m_{\max}$ sector such that only eigenvalues with $s = m_{\max} - 1$ remain. With this, we have extracted all energies of the $s = m_{\max} - 1$ sector. This idea is visualized in figure 9.

We can continue this procedure for further values of m to find the entire set of correct assignments for s. Still, there are a few issues to address. First of all, due to the degeneracy of the s states, denoting the state with an s and an m label may be confusing. As an example, the $s = 4, m = 1$ sector contains the same energies as the e.g. $s = 4, m = 0$ sector or the $s = 4, m = 4$ sector. Clearly, we only have to consider one of those degenerate sectors and we can decide how to label them. For

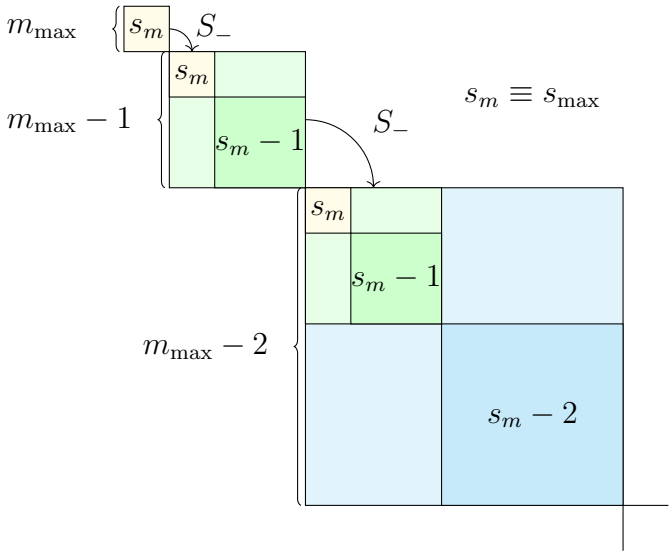

Figure 9: Schematic sketch of the implementation of the S^2 symmetry. Because of the commutation of H and $S_\pm$ we find the eigenvalues of the m sector in the $m-1$ sector. Extracting those yields us the $s = m - 1$ sector.

the remaining thesis we usually write $s = m$. Still, it is important to remember that we could also write it with a different value for m while finding the same statistics.

Secondly, the order in which we identify the eigenvalues of the sectors is important. In the normal procedure described above we start with the maximal m sector and continue identifying all lower sectors one after another. Yet, it may be the case that we are only interested in a specific s sector. Having to go through all m until we reach $m = s$ is quite tedious. In this case it is more efficient to just identify all eigenvalues of the $m = s + 1$ sector in the $m = s$ sector. Here it is essential that we use the $m = s + 1$ sector as a whole, as it already includes all the eigenvalues of all unwanted s sectors above.

3.4.2 η-Pair Symmetry

The η-pair symmetry shares the same SU(2) commutation relations as we know from the spin algebra for the operators η^2, η_z and $\eta_\pm$. However, a major difference are the commutation relations with the Hamiltonian. While η^2 and η_z both commute with H making them symmetries of the system, the ladder operators $\eta_\pm$ do not commute with H. This makes sense, as $\eta_\pm$ creates or annihilates pair states containing a pair of a spin up and down particles. These pairs yield a contribution to the interaction. Therefore, the ladder operators cannot commute with the interaction term of the Hamiltonian. Recall from equation (2.19) the commutation relation

$$[H, \eta_\pm] = \pm U \eta_\pm.$$

This results in a problem as we loose the feature of the degenerate energies we have found for the spin algebra. Nevertheless we find a similar solution. Let us again

consider a state $|\xi, \tilde{n}\rangle$ with energy $E_{\xi,\tilde{n}}$. Acting with the ladder operator η_- on this state yields $|\xi, \tilde{n}-1\rangle$. Using the commutation relation we find for this state the energy $E_{\xi,\tilde{n}\pm1} = E_{\xi,\tilde{n}} - U$. Thus, even though we do not have degenerate energies they are only differing by a constant shift of U. Moreover, we note that this shift cancels when calculating the level statistics by taking the level spacings. As a consequence for a given ξ the available $\tilde{n}$ sectors yield the same level statistic distribution.

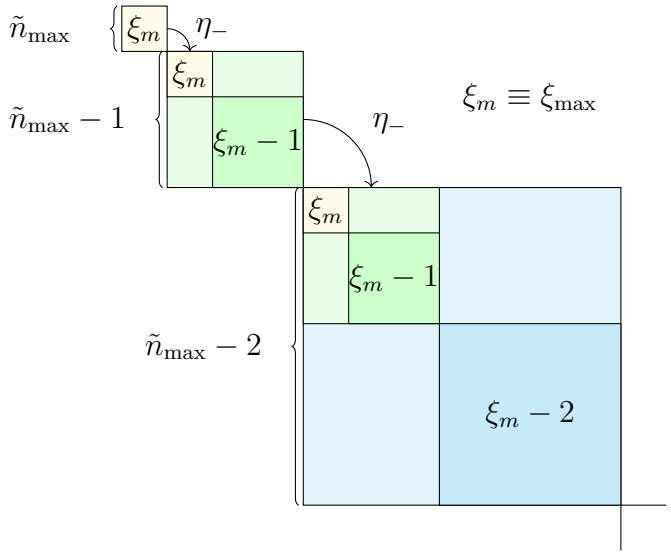

Figure 10: Schematic sketch of the implementation of the η^2 symmetry. Because of the commutation of H and $\eta_\pm$ we find the eigenvalues of the $\tilde{n}$ sector shifted by U in the $\tilde{n}-1$ sector. Extracting those yields us the $s = \tilde{n} - 1$ sector.

The basic approach when implementing this symmetry is almost the same as for the spin symmetry. We begin with the highest $\tilde{n}$ sector and find the energies subtracted by U in the $\tilde{n}-1$ sector. The remaining eigenvalues form the $\xi-1$ sector. Continuing this procedure yields us any ξ sector. The procedure is depicted in a similar manner as before in figure 10. Note that in reality we only consider e.g. the sector with $\tilde{n}-1$ corresponding to $N-2$ and extract it as a whole instead of considering all the $\tilde{n}$ sectors. For more details on this symmetry's behaviour we refer to appendix B.

3.5 Overview

Let us summarize the procedure to generate the spectrum of an $N, s, m', k, (p), \xi_{\min}$ subsector as displayed in figure 11. Note, that we restrict ourselves without loss of generality to the cases of $N \leq L$ and recall that due to degeneracies, the choice of m' is arbitrary. First, we conduct an exact diagonalization in which we find a simultaneous eigenbasis and diagonalize the symmetry blocks. For this we begin with generating all position basis states with a fixed number of particles and spin z-component. Here the m coincides with s later. Next, we consider the spatial symmetries. If $k' \neq 0, \pi$ we find all representatives for the translation symmetry and save the coefficients of the eigenstates. In the other case we have to additionally consider the reflection symmetry

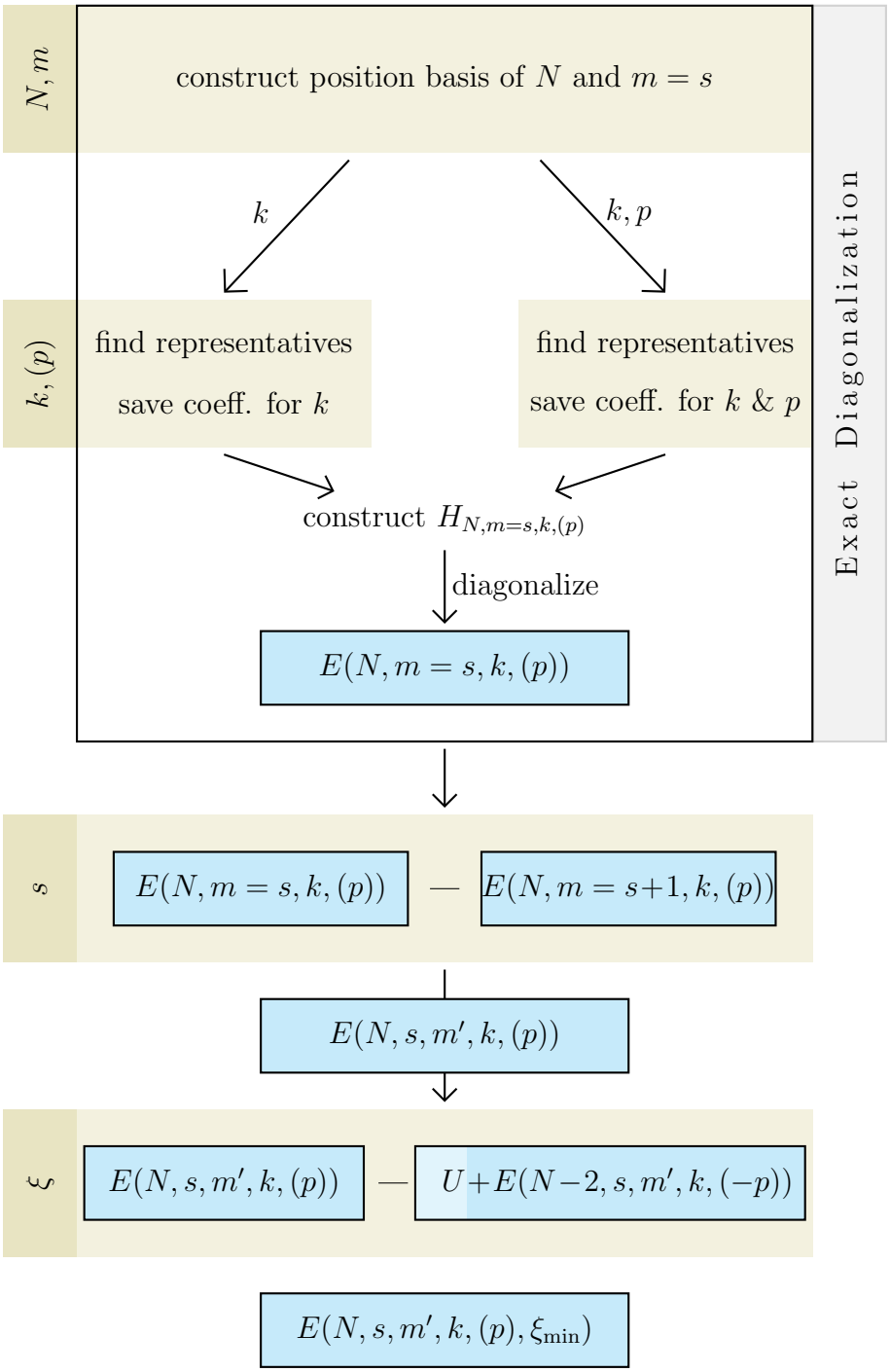

Figure 11: Overview of the process of generating the spectrum of a symmetry subsector $N, s, m', k, (p)$. Note that m' can be chosen arbitrarily because of the energy degeneracy in the sectors for fixed s. We start the procedure with an exact diagonalization in which we first implement the N and m conservation as well as the spatial symmetries with k and p if available. This enables us to diagonalize the Hamiltonian for a symmetry block. After this, the total spin and pseudospin are implemented taking advantage of their relation to other sectors.

when finding the representatives and coefficients. Using the obtained representatives we can generate the block matrix $H_{N,m=s,k,(p)}$ of the symmetry sector. The last step is given by the diagonalization that yields us the energies for the $N, m = s, k, (p)$ subsector.

The two remaining symmetries are implemented utilizing other subsectors spectra. For the total spin s we find the degenerate energies with the $N, m+1, k, (p)$ sector and extract the remaining energies. This yields the $N, s, m', k, (p)$ sector. For the total pseudospin ξ we perform a similar procedure. Every energy in the $N-2, s, m', k, (-p)$ subsector is shifted by U and then eliminated in our original sector. As a result we obtain the desired $N, s, m', k, p, \xi_{\text{min}}$ subsector.

3.5.1 Specifications of the Exact Diagonalization

Let us shortly summarize some details about the capabilities of the written exact diagonalization. The exact diagonalization yields the eigenvalues of the dimerized Hubbard model assigned to the conserved quantities N, m, k and p. As the reflection is only present for some momenta, the fully diagonalisable system size is limited by the amount of energies in the N, m, k sectors.

For the number of states in a L, N, m, k sector we find the equation [WF08]

$$M(L, N, m) = \binom{L}{N_\uparrow}\binom{L}{N_\downarrow}\frac{2}{L} = \binom{L}{N/2+m}\binom{L}{N/2-m}\frac{2}{L}, \tag{3.2}$$

where we assume that the states are equally distributed in the momentum sectors.

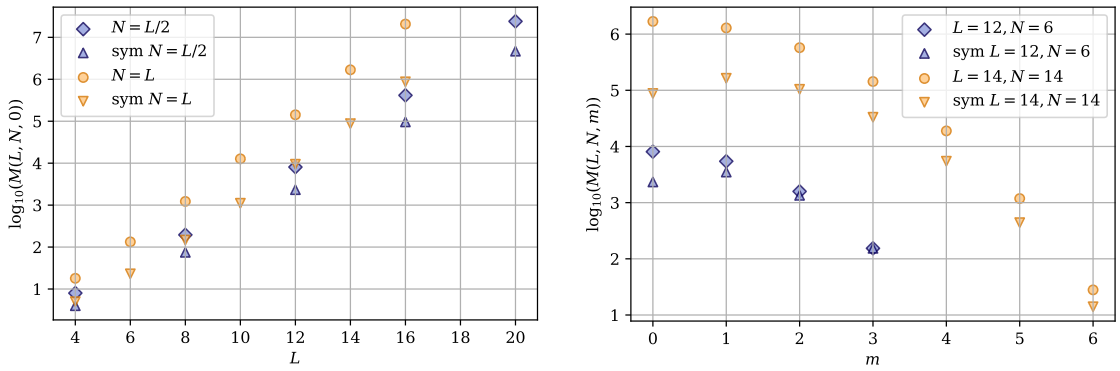

Figure 12: Decadic logarithm of number of states in a symmetry sector N, k, m and $N, k, s = m, \xi$. We compare half filling and quarter filling for $m = 0$ in dependence of the system size L (left hand figure) or for two system sizes L in dependence on m (right hand figure). We observe that the order of the number of states rises almost linearly. For the spin sectors we also find an increase of states contained for spins closer to zero. However, taking all symmetries into account, we find that the $m = 1$ sector becomes largest in size.

The number of states M is displayed logarithmically in figure 12 in dependence on the system size L and spin m for different fillings. Furthermore, the number of

states in each sector also considering s and ξ is depicted for comparison. For this we subtract the number of states in the $N-2$ and $m+1$ sector in accordance to the implementation of these symmetries.

In figure 12 we observe that the order of magnitude of the number of states almost grows linearly with system size L. Considering the additional symmetries notably decreases the number of states in a sector. For different spins m we find that the highest number of states is in the $m=0$ sector. However, after considering all symmetries the $m=s=1$ sector becomes largest.

L	N	m	k	p	size
12	6	0	1	–	8064
16	8	3	1	–	22880
12	12	3	1	–	8064
14	14	4	1	–	18928
14	7	1.5	1	–	26026
14	7	0.5	0	1	26026

Table 1: Number of eigenvalues in symmetry subsectors after exact diagonalization. Note that all momentum sectors contain the same number of energies. If the reflection symmetry is also present, the number of energies is halved for these subsectors.

A variety of other subsectors with the number of eigenenergies are listed in table 1. One of the largest sectors that were possible to generate are the $L=16, N=8$, $m=3, k$ sectors. The individual subsectors contain about 23000 eigenvalues and achieved an accuracy of 11 digits.

The most limiting factor of the exact diagonalization routine is given by the required memory. Solely, the allocation of a 20000×20000 matrix of complex floats requires at least $2 \cdot 4 \cdot 10^8 \cdot 64\,\text{bit} = 6.4\,\text{Gb}$ of memory. As this does not include the diagonalization as well as the construction of the basis and the matrix, the required memory can become about 15 Gb for the largest available sectors.

From this, it becomes clear that the mere size of the matrices prevents us from generating sectors which contain more than about 10^5 states. Implementing the remaining S^2 and η^2 symmetry directly into the exact diagonalization would allow us to generate a few of the higher sectors by decreasing the number of states. However, with this we only gain an insight into the spectra of slightly larger system sizes.

4 Level Statistics of the Dimerized Hubbard Model

Now that we have discussed a way to generate the spectrum divided into the symmetry subsectors we will consider the level statistics. First, we have a look at the influence of the symmetries on the level statistics. Secondly, a specific analytically solvable subspace given by the non-interacting sectors is introduced. As we expect these symmetry subsectors to be integrable, we consider the level statistics separately. After this, we continue with the discussion of the general properties of the level statistics for quarter and half filling. To gain an understanding of the dependence on the parameters t'/t and U/t of the model and the tendency of the thermodynamic limit we vary the two parameters of the system independently for different system sizes. Moreover, we are going to compare the results for the dimerized Hubbard model with the ionic Hubbard model.

4.1 Influence of Symmetries on the Level Statistics

As discussed in section 2.2, it is vital to know all simultaneously present symmetries of the model in order to analyse the level statistics. Only if the level statistics are considered of eigenvalues which belong to one complete set of conserved quantities, we can observe the GOE distribution characteristic for a chaotic model. Taking all eigenvalues of different symmetry sectors into account might lead to a Poisson distribution. This might mislead us into concluding the model to be integrable. To further illustrate this statement we consider the level statistics for the dimerized Fermi Hubbard Model with a different number of symmetries respected. Note that after calculating the ratios for the respective symmetry sectors, the distributions are merged.

The histograms of $P(r)$ are displayed in figure 13 and compared to the distribution expected for the GOE or Poisson case. We use the $L = 16$, $N = 8$ and $m = 3$ sector. As we have already established k, p, s and ξ are the remaining conserved quantities we expect for this model. Since the division into these subsectors is still missing, we find many degenerate energies in this sector which equivalently results in zero level spacings and ratios. Thus, a dominating peak at zero in the $P(r)$ histogram emerges. For the sake of readability, we neglect this peak only in figure 13a by deleting all vanishing level spacings.

The resulting plot still exhibits a smaller peak stemming from very small level spacings. Besides this, we note how the distribution $P(r)$ resembles a Poisson distribution. Hence, at this point we could come to the conclusion that the model is integrable. However, if we now also respect the translation symmetry as shown in figure 13b the histogram drastically changes. The distribution becomes more similar to the GOE distribution with a shift to smaller ratios. This shape is characteristic for a superposition of independent GOE sectors. A peak at zero is still noticeable.

By also dividing the energies into the subsectors of the quantities p and s as in figure 13c, the distribution now fits the general GOE shape. In order to resolve the remaining degeneracies, the symmetry with conserved quantity ξ is necessary which can be seen in figure 13d. Within the symmetry block the level statistics satisfy the prediction of the GOE case. Hence, already neglecting only some of the symmetries

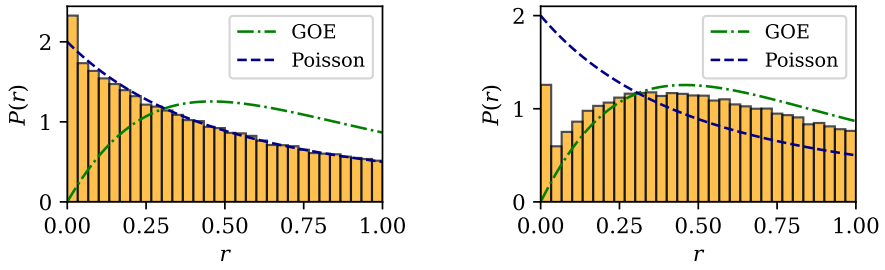

(a) No additional symmetry

(b) Respecting k

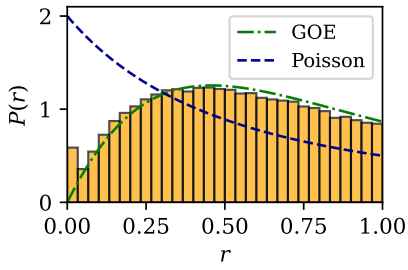

(c) Respecting k, p, s

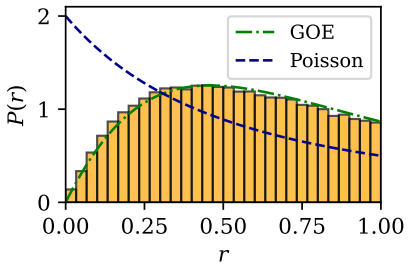

(d) Respecting k, p, s, ξ

Figure 13: Distribution of ratios $P(r)$ for different sets of symmetries respected. In all cases $L = 16, N = 8$ and $m = 3$ for $t'/t = 2, U/t = 2$. Note that in 13a a large number of degenerate values resulting in a peak at zero were neglected for readability. We observe the importance of considering all symmetries.

as in figure 13a would lead to the model being falsely labelled as integrable as it fits the shape of a Poisson distribution.

4.2 Non-interacting Sectors

Before continuing with the general analysis of the properties of the level statistics, we are going to introduce two special cases. These cases are characterised by being non-interacting and, thus, specific symmetry sectors of the dimerized Hubbard model which are analytically solvable. Therefore, we expect a Poisson distribution. In reality, we observe neither with the data.

Let us first clarify which cases are affected. It is obvious that for $U = 0$ the model is non-interacting. Additionally, the sectors with maximal (absolute) spin S_z are effectively non-interacting. This is a mere consequence of having maximal total spin resulting in all particles being in one spin state, such that the interaction is not acting. Hence, even for $U \neq 0$ we already find a non-interacting and, consequently, non GOE like subsector.

The $P(r)$ histogram of such a non-interacting sector is shown in figure 14. As an example we have chosen $U = 0$ for $L = 12$ sites at quarter filling and vanishing spin. Recall, that the filling is defined to be the number of particles per twice the number of sites $n = N/(2L)$. Similarly to the case of figure 13a we find a dominant peak

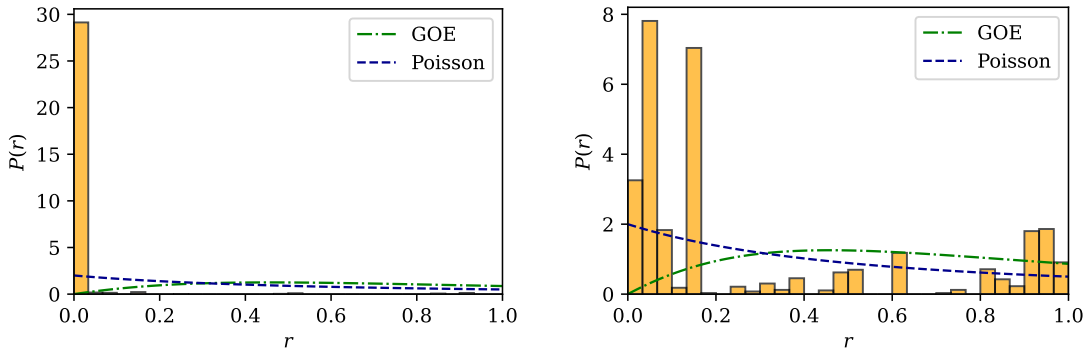

Figure 14: Distribution of ratios $P(r)$ for a non-interacting case with $U/t = 0$ and $t'/t = 2$. The sector $L = 12$, $N = 6$, $s = m = 0$ with was used. On the left hand side an unedited version is displayed. For the sake of readability the peak at zero was omitted in the right hand side figure.

at zero. Again, this is a consequence of the a overwhelming amount of degeneracies. However, neglecting these contributions does not yield a Poisson distribution. This is not a novelty. Already in the original paper introducing the Poisson distribution for integrable systems the harmonic oscillator with commensurate frequencies yielded an exception [BT77]. The problem here is likely to be found in the triviality of the solutions for the non-interacting model. As the solution of the many-body non-interacting model is a superposition of the single particle solutions (Appendix A), the energy spectrum consists of sums over the single particle energies. Therefore, we find an intrinsic amount of degeneracies and no Poisson like distribution. Other works elaborating this topic for the harmonic oscillator are [PBG89; PR91].

As we already know that these sectors are integrable it is not our aim to further investigate this. Therefore, we are going to ignore the non-interacting sectors and keep in mind that in the non-interacting limit we expect largely deviating distributions from the Poisson predictions for our considered set of conserved quantities.

4.3 Dependence on Spin

In the histograms of $P(r)$ we have seen so far, all of the symmetry subsectors distributions are merged for a given L, N, ξ and $s = m$, i.e. all available k and p sectors are combined after calculating the ratios. We do not expect severe differences in the behaviours of the k and p sectors such that combining them only increases the amount of data and, thus, decreases the relative statistical fluctuations. Is there a reason to not merge the sectors for ξ or $s = m$ and if not, which sector do we choose when considering them?

For the quantity ξ the explanation is straightforward. In general, we are interested in the statistics for a certain system size L with a particle number N. If we choose ξ not minimal in this sector, we find an equivalent level statistic for particle number $N - 2j$ case with $j \in \{1, 2, \ldots, N/2\}$(see Appendix B). This opposes the idea of

considering a fixed filling. Therefore, for the remaining analysis we always consider ξ_{min}.

For the spin quantities the discussion is not as easy. We are not always able to obtain the data for the desired spin s by the limitations of our exact diagonalization. Therefore, we are shortly discussing the influence of the spin conserved quantities $s = m$ on the level statistics.

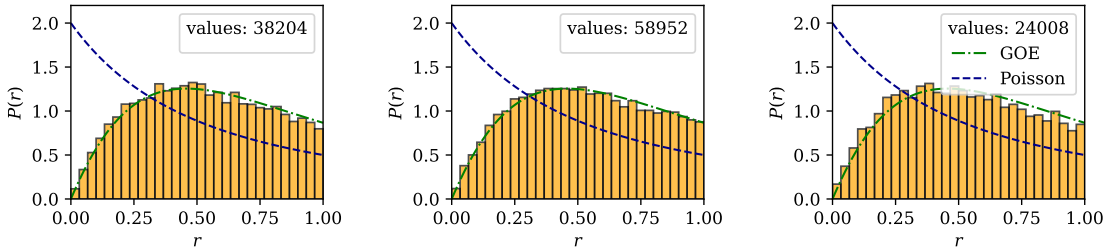

(a) $s = m = 0$, $\langle r \rangle = 0.527$ (b) $s = m = 1$, $\langle r \rangle = 0.53$ (c) $s = m = 2$, $\langle r \rangle = 0.518$

Figure 15: Distribution of ratios $P(r)$ for $L = 14$, $N = 6$ with $t'/t = 2$ and $U/t = 2$ for different spins $s = m$. For all parameters the k, p sector statistics are merged and we use $\xi = 4$.

For this we generate the distribution of ratios $P(r)$ for $L = 14$ and $N = 6$ for $s = m \in \{0, 1, 2\}$ as it contains a relative high number of energies in these spin sectors and is close to quarter filling. These are depicted in figure 15. Moreover, the mean values calculated for the distribution of ratios from equation (2.9) are provided. We observe that the lower spin sectors both look very similar and close to GOE. The highest shown spin sector $s = 2$ shows smaller deviations also visible in the mean ratio. Still we cannot identify larger differences.

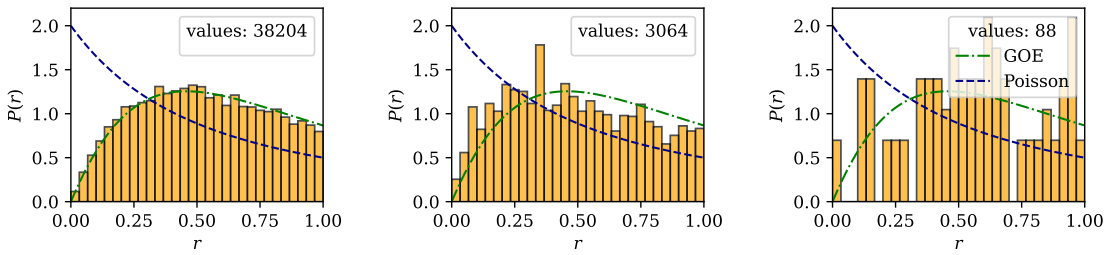

(a) $s = m = 4$, $\langle r \rangle = 0.527$ (b) $s = m = 5$, $\langle r \rangle = 0.488$ (c) $s = m = 6$, $\langle r \rangle = 0.555$

Figure 16: Distribution of ratios $P(r)$ for $L = 14$, $N = 14$ with $t'/t = 2$ and $U/t = 2$ for different spins $s = m$. For all parameters the k, p sector statistics are merged and we use $\xi = 0$.

As a comparison, let us consider the distribution $P(r)$ for $L = 14$ and $N = 14$ for $s = m \in \{4, 5, 6\}$ in figure 16. Lower spins were not possible to generate with the used diagonalization routine. In this case we observe for the lowest available

spin $s = 4$ a GOE behaviour while the results for the $s = 5$ sectors clearly deviate from it. Even though the number of energies in the sectors decreases rapidly for half filling these deviations seem unlikely to solely originate from statistical fluctuations. Another problem may be finite size effects that seem to be more present in higher spin sectors. The $s = 6$ sector contains very few energies making it not informative. Still, we encounter degeneracies in the $s = 6$ sector which should not be the case for a GOE like sector.

Thus, it is in general not reasonable to combine all spin sectors. Especially, for half filling the spin may influence the result for the distribution $P(r)$ even possibly leading into degeneracies for larger spins. Regarding the latter problem, it is likely to be an effect vanishing for increasing system sizes as we find the degeneracies in smaller systems for even smaller spins s. They may originate from the influence of the non-interacting and, thus, integrable maximal spin $s_{\max}$ sector.

However, for other fillings we find that the lowest spin sectors $s = 0, 1$ coincide with the GOE distribution the most while larger spin systems exhibit minor deviations. As a consequence, to decrease statistical fluctuations it might be useful to combine few spin sectors with low spin values. Moreover, when we are obliged to use $s \neq 0$ sectors for the analysis, it yields us a lower estimate on the results of the $s = 0, 1$ sectors.

4.4 Dependence on Hopping Amplitude

Next, we are going to consider the properties of the level statistics for different hopping amplitudes. For this, we calculate the mean ratio $\langle r \rangle$ as in equation (2.9) of the distribution of ratios $P(r)$.

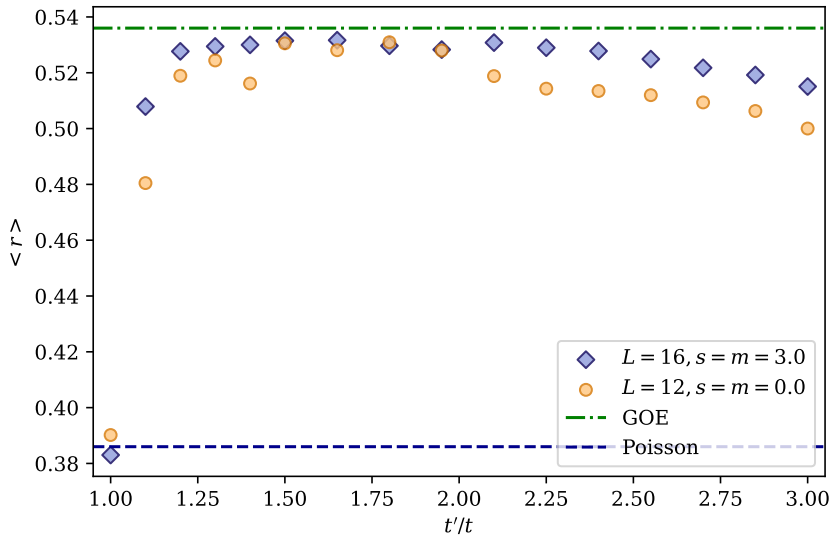

Figure 17: Mean values of the distribution of ratios $P(r)$ for quarter filling depending on the hopping amplitude t'/t with $U/t = 2$. For both system sizes the k, p sector statistics are merged and we use $\xi = 3$ and $\xi = 4$ for $L = 12$ and $L = 16$ respectively. We observe a convergence towards the GOE mean ratio and finite size effects.

First, we consider two different system sizes, $L = 12$ and $L = 16$ for quarter filling in figure 17. The interaction is kept constant at $U/t = 2$. Let us analyse how the mean ratios generally evolve. For $t'/t = 1$ we are in the limit of the Fermi Hubbard Model. We already know that it is integrable, hence, we expect a Poisson distribution. The mean ratios confirm this very well. Increasing the hopping amplitude results in a slow convergence towards the ratio expected for the GOE distribution. After remaining close to this value for a while, we observe a decline again. Therefore, at least for an interval of the hopping amplitude, the level statistics exhibit the GOE predictions.

Still the question remains how to classify the behaviour beyond this interval. Therefore, we consider the distributions between the Poisson and GOE case for small deviations from the Fermi Hubbard model limit. Distribution of ratios histograms for different values of t'/t are displayed in figure 18 for $L = 16$. Here for $t'/t = 1$ the Poisson distribution can be seen very well, whereas for hopping amplitude $t'/t = 1.1$ it is almost completely shifted towards a GOE distribution. In between for $t'/t = 1.05$ we observe a distribution that neither fits Poisson nor GOE distribution well. Note that even though the hopping only has a small deviation from the Fermi Hubbard limit, the number of small ratios has drastically decreased.

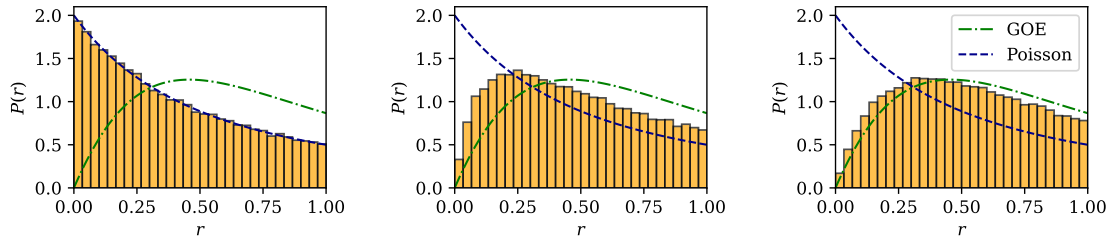

(a) $t'/t = 1$ (b) $t'/t = 1.05$ (c) $t'/t = 1.1$

Figure 18: Distribution of ratios $P(r)$ for different hopping amplitudes. For all histograms $L = 16$, $N = 8$, $s = m = 3$, $\xi = 4$ the ratios were calculated in k, p sectors and merged. For this set of hopping amplitudes we can see the shift between the Poisson limit towards a GOE distribution.

The most probable explanation for the distribution of ratios neither fitting to GOE nor to Poisson values in this regime is the finite size of the system. Following this idea, in the thermodynamic limit $L/N \to \infty$ these mean ratios are expected to converge to the GOE case for this model. To verify this tendency we compare two different system sizes in figure 17. Two major features can be pointed out. First of all, the mean ratios exhibit a steadier evolution for the larger system size. An explanation for this is given by the larger amount of data given for this system. As a result, also the statistical fluctuations decrease. Secondly, the larger system size converges faster to the GOE case and declines later. This is an important indicator towards the finite size explanation.

The level statistics for $t'/t = 1.05$ and $t'/t = 1.1$ are going to serve well to examine the finite size effects as it catches the intermediate behaviour and a regime close to GOE. Therefore, we compare this case for three different system sizes $L \in \{8, 12, 16\}$

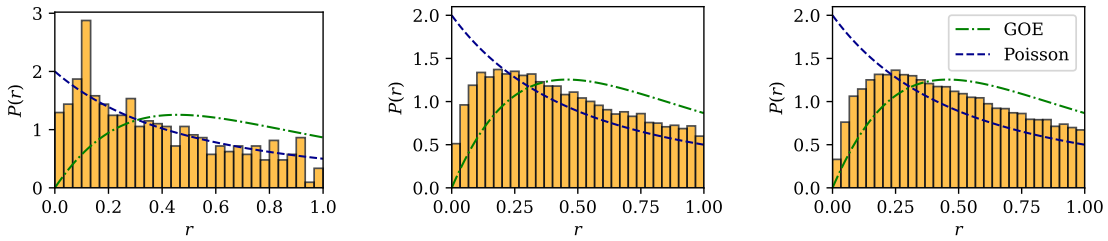

(a) $L = 8$, $N = 4$ (b) $L = 12$, $N = 6$ (c) $L = 16$, $N = 8$

Figure 19: Distribution of ratios $P(r)$ for different system sizes. Histograms are made for $t'/t = 1.05$ and $U/t = 2$. Moreover, all available (interacting) spin $s = m$ sectors and k, p sectors are merged. We observe the finite size effect in the regime between Poisson and GOE.

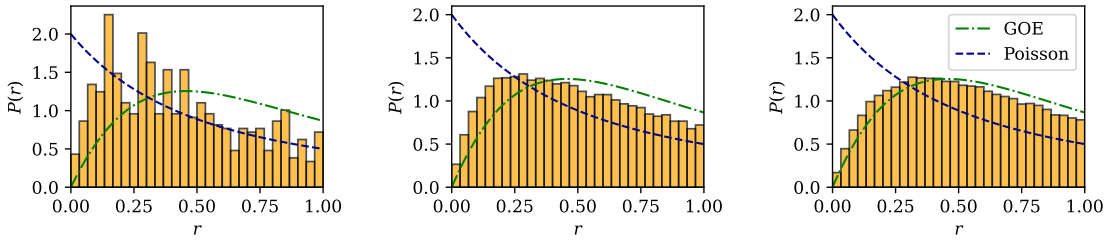

(a) $L = 8$, $N = 4$ (b) $L = 12$, $N = 6$ (c) $L = 16$, $N = 8$

Figure 20: Distribution of ratios $P(r)$ for different system sizes. Histograms are made for $t'/t = 1.1$ and $U/t = 2$. Moreover, all available (interacting) spin $s = m$ sectors and k, p sectors are merged. We observe the finite size effect in the regime where larger system sizes are close to GOE behaviour.

for quarter filling in figure 19 for $t'/t = 1.05$ and in figure 20 for $t'/t = 1.1$. Note that for the two smaller system sizes all of the available spin sectors are merged in order to suppress the statistical fluctuations.

First, we focus on the larger systems with $L = 12$ and $L = 16$. For $t'/t = 1.1$ we observe how the larger system size $L = 16$ is closer to the GOE behaviour. For $t'/t = 1.05$, even though the distribution of ratios for $L = 12, 16$ look similar there are minor differences. For $L = 12$ the amount of small ratios is larger. Moreover, for bigger ratios the histogram fits closer to the Poisson distribution even though it is difficult to notice. Overall, we observe for $L = 16$ a histogram closer to the GOE distribution than for the $L = 12$ case. Now comparing the smallest system size $L = 8$ with the remaining, the difference is even more noticeable. Neglecting the severe statistical fluctuations we find a histogram fitting well to the Poisson case for $t'/t = 1.05$ with the exception of small ratios where we can suspect the tendency towards a GOE behaviour. For the larger hopping amplitude $t'/t = 1.1$ the distribution of ratios deviates more from the Poisson like behaviour but is still clearly differing from the GOE predictions. Therefore, it also agrees with our expectations of the finite size

effects.

Hence, for these sets of parameters we observe that the finite size has indeed an influence on the level statistics. The distributions converge towards a GOE behaviour with growing size. However, we also note that comparing the differences for the system sizes $L = 12$ and $L = 16$ we have to expect a very slow convergence. Still, as the considered system sizes are relatively small in comparison to the thermodynamic limit and, moreover, the considered hopping is close to the Poisson case, this is not unreasonable.

With this consideration of the finite size effects we conclude the discussion for the quarter filling dependence on the hopping amplitude. We observed that by increasing the system size L, the values of distributions get closer to the GOE prediction. As we have only explored the behaviour for one filling so far, we continue with the level statistics for half filling. Again, to visualize the dependence on the hopping amplitude, we compute the mean ratios which are depicted in figure 21.

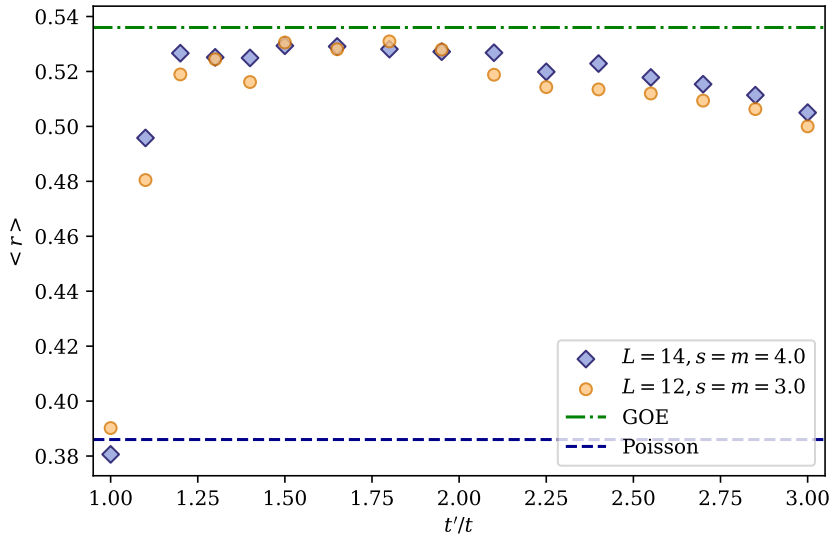

Figure 21: Mean values of the distribution of ratios $P(r)$ for half filling in dependence on the hopping amplitude t'/t with $U/t = 2$ fixed. For both system sizes the k, p sector statistics are merged and we use $\xi = 0$. We can observe a convergence towards the GOE mean ratio and partly finite size effects.

We find a similar behaviour as before. For $t'/t = 1$ we observe a Poisson mean ratio as expected. Again the mean ratios converge to the GOE case and deviate after some time. Beyond the interval of nearly converged GOE behaviour the finite size effects are again notable. The mean ratios for the larger system size $L = 14$ are closer to the GOE values than for the smaller system size $L = 12$.

4.5 Dependence on Interaction

Next, we keep the hopping amplitude t'/t fixed while considering the dependence on the interaction U/t. The mean value of the distributions $P(r)$ for quarter filling systems are depicted in figure 22 and for half filling in figure 23. As discussed in subsection 4.2 we omit the ratios for $U/t = 0$.

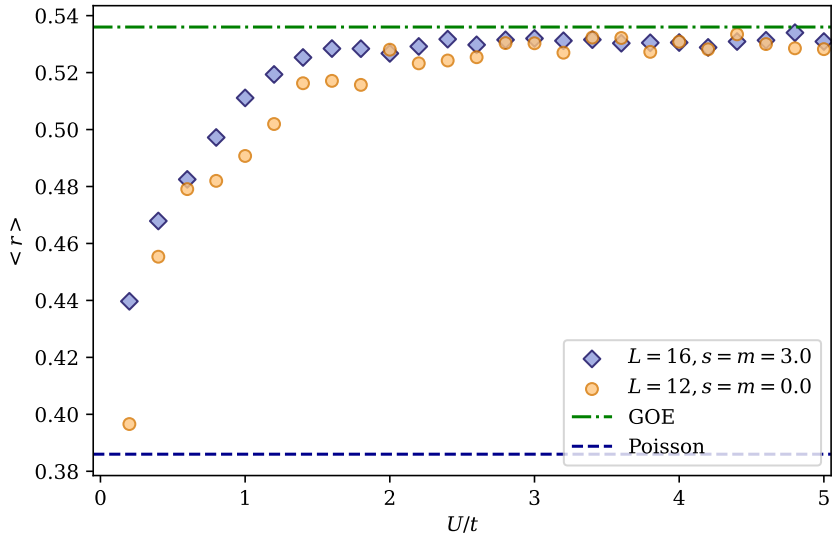

Figure 22: Mean values of the distribution of ratios $P(r)$ for $L = 12, 16$ for quarter filling in dependence on the interaction U/t with $t'/t = 2$. For both system sizes the k, p sector statistics are merged and we use $\xi = 3$ and $\xi = 4$ for $L = 12$ and $L = 16$ respectively. We can again observe a convergence towards the GOE mean ratio.

In general we can observe the same behaviour as before. For increasing U/t the mean values slowly converge towards the GOE expectations. For quarter filling the bigger system size converges typically faster, again supporting the finite size explanation. Even though in the half filling case a small number of ratios of the smaller system size surpass the larger sizes values, we find a similar finite size behaviour. As we still find notable statistical fluctuation in the $L = 12$ system due to its size and the difference between the two compared system sizes is smaller than for the quarter filling case, this yields no serious problem.

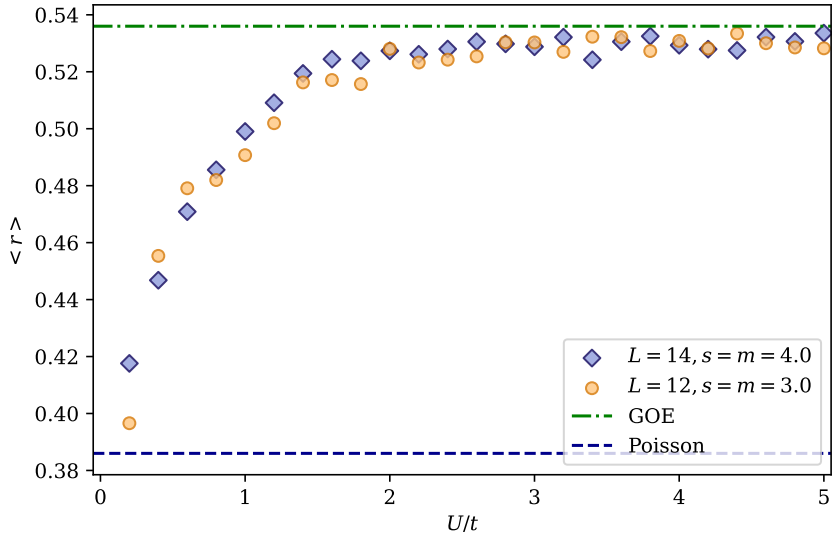

Figure 23: Mean values of the distribution of ratios $P(r)$ for $L = 12, 14$ for half filling in dependence on the interaction U/t with $t'/t = 2$ fixed. For both system sizes the k, p sector statistics are merged and we use $\xi = 0$.

4.6 Comparison to the Ionic Hubbard Model

Since a level statistic analysis has been conducted for the ionic Hubbard model in [De +22], we compare the results of the two models with each other. The general outcome for both models is similar. Except for the Fermi Hubbard case when $\mu/t = 0$ in the ionic Hubbard model in equation (2.12) or $t'/t = 1$ for the dimerized Hubbard model in equation (2.13) we find GOE behaviour neglecting the finite size effects. For comparison two figures containing the dependence of the mean ratios are shown in figure 24.

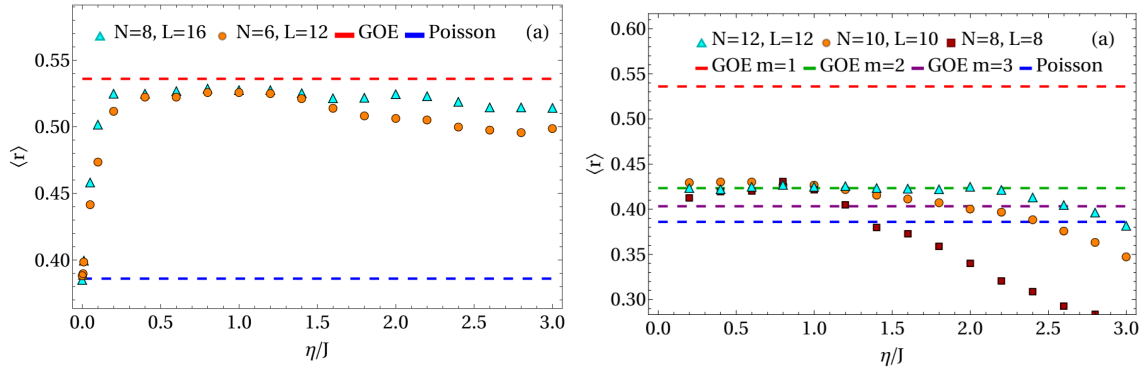

Figure 24: Mean values of the Distribution of ratios $P(r)$ for the ionic Hubbard model in dependence of the potential η/J (μ/t) for fixed interaction $U/J = 2$ in the left figure and $U/J = 1$ for the right figure. Note that in general all spin sectors $s = m$ are additionally combined if possible. Figures taken from [De +22].

Note that we have to expect the influence of the potential μ from equation (2.12) to scale differently than the hopping amplitude t'. Still, comparing with the equivalent figure 17 of the dimerized Hubbard model we find a similar convergence to the GOE mean ratio in an interval. Therefore, in this case the two models yield the same behaviour.

For half filling the particle hole symmetry was missing in the ionic Hubbard model. Therefore, the mean ratios do not converge towards the GOE expectation but a superposition of two equal size GOE sectors. As for the dimerized Hubbard model this symmetry is included in the η-pair symmetry, we do not observe this behaviour.

4.7 Summary

Our analysis has shown us different aspects of the properties of the level statistics. We find few integrable non-interacting subsectors next to the integrable limit of the Fermi Hubbard model for $t = t'$. For the remaining regime we observe a convergence towards a GOE distribution when considering the distribution of ratios for different parameters. Still, for finite size an intermediate behaviour is visible but comparison of different system sizes suggests even in these regimes a convergence towards the GOE case in the thermodynamical limit.

5 Conclusion

The aim of this thesis was to examine the dynamical features of the dimerized Hubbard model. We were interested whether we can expect the system to thermalize which is closely linked to the spectral properties of the model. This led us to the level statistics that require a profound understanding of the symmetries present.

We found that there are four known different symmetries simultaneously present for the dimerized Hubbard model. These are the two spatial symmetries, namely the translation and reflection symmetry, and two SU(2) symmetries, the spin and η-pair symmetry. Together, they yield the conservation of momentum k, parity (p), total spin s, spin z-component m, total pseudospin ξ and pseudospin z-component $\tilde{n}$ where we have often used the total particle number N instead of $\tilde{n}$.

After this we introduced a method to generate the spectrum respecting these symmetries, i.e. the spectrum of each symmetry subsector. For the quantities k, p, m and N we used an exact diagonalization utilising the common eigenbasis of the corresponding symmetries. The two remaining conservations of s and ξ were implemented by taking advantage of the commutation relations between the ladder operators and the Hamiltonian. This led to a procedure where various other symmetry sectors were used to extract the correct spectrum for these quantities.

Finally, we analysed the properties of the level statistics. On the one hand, we found sectors exhibiting Poisson statistics. This contains the Fermi Hubbard case with equal hopping amplitude $t = t'$ and the non-interacting sectors with $U = 0$ or maximal magnetization m_{max}. For the other sectors we partially found GOE statistics. For the parameters where neither Poisson nor GOE statistics were fulfilled, we observed the convergence towards the GOE case with increasing system size. When neglecting these finite size effects in the thermodynamic limit, we can expect to find a GOE distribution in general. Thus, in these subsectors we expect thermalization.

Still, there are various topics to explore. At the moment our analysis is limited by the symmetry subsector spectrum we can generate using the exact diagonalization. Adding the total spin s conservation to the exact diagonalization would enable us to explore larger system sizes and further confirm the finite size effects that were indicated here.

The η-pair symmetry was an unexpected symmetry we have found present in the dimerized Hubbard model. Due to the properties of the spectrum generating algebra it might be of interest to study the associated dynamics. It remains to determine, in which way these states having equidistant energies influences the time evolution.

Moreover, now that both the ionic and dimerized Hubbard model are analysed for thermalization, we can continue considering other models, e.g. a combination of both. This will pose new challenges since two of the symmetries, the reflection and η-pair symmetry, are broken.

In conclusion, we have conducted a theoretical groundwork for exploring the dynamical properties of the dimerized Hubbard model. Our analysis of the spectral properties has shown GOE characteristics in the symmetry subsectors. As a consequence, in these subsectors thermalization may be expected. A confirmation of this behaviour or of other dynamical effects is still a topic for future research.

Acknowledgements

I would like to thank my supervisor Prof. Corinna Kollath for giving me the opportunity to write my master thesis in her group. I am grateful for the support and discussions over the last months. Moreover, I very much appreciate the supervision provided by Ameneh Sheikhan and thank for the countless discussions. If I had questions of any kind, she always offered a helping hand. I also want to mention the other members in our group as they have always shown great support and made the time very enjoyable. Especially, I thank Luisa Tolle for providing me help for the general topic and the BAF Cluster, I was initially very overwhelmed with. Furthermore, I am very thankful to Prof. Dr. Hartmut Monien for becoming the second supervisor of this thesis.

Besides the university, Stephan Roschinski was always open for a conversation about my work. He, next to Margarita Gerl, Konstantin Mauer, Astrid Haderlein and Jan Thomm were willing to proofread my thesis and provide me with valuable feedback. Moreover, I would like to thank my family for the continuous support over the last years making this thesis possible. And lastly, I cannot express my appreciation towards Jan Thomm for always being by my side while always trying his best to help and support me.

Appendix

A Energy Levels of the Non-Interacting Dimerized Hubbard Model

The non-interacting dimerized Hubbard Hamiltonian takes the form

$$H = -t \sum_{\sigma} \sum_{\substack{j=1 \\ \text{odd}}}^{L} c_{j\sigma}^{\dagger} c_{j+1\sigma} - t' \sum_{\sigma} \sum_{\substack{j=1 \\ \text{even}}}^{L} c_{j\sigma}^{\dagger} c_{j+1\sigma} + \text{h.c.}$$

where t and t' denote the alternating hopping amplitudes and h.c. is an abbreviation for the hermitian conjugate.

We calculate the one particle energy levels and afterwards construct the many particle energies by adding those. This is possible as the model is non-interacting and the particles can be considered as free particles.

Therefore, we start by redefining the creation and annihilation operators. Note that because of the different hoppings t and t', we find a bipartite lattice structure. Hence, we choose different operators for particles on even or uneven sites which we define by

$$c_{j\sigma}^{\dagger} = \begin{cases} a_{j\sigma}^{\dagger} & j \text{ odd} \\ b_{j-1\sigma}^{\dagger} & j \text{ even} \end{cases}.$$

Plugging this into the Hamiltonian we obtain

$$\begin{aligned} H &= -t \sum_{\sigma} \sum_{\substack{j=1 \\ \text{odd}}}^{L} a_{j\sigma}^{\dagger} b_{j\sigma} - t' \sum_{\sigma} \sum_{\substack{j=1 \\ \text{odd}}}^{L} b_{j\sigma}^{\dagger} a_{j+2\sigma} + \text{h.c.} \\ &= -t \sum_{\sigma} \sum_{j=1}^{L/2} a_{j\sigma}^{\dagger} b_{j\sigma} - t' \sum_{\sigma} \sum_{j=1}^{L/2} b_{j\sigma}^{\dagger} a_{j+1\sigma} + \text{h.c.}, \end{aligned}$$

where we have used in the last step that all indices are odd and we can shift the summation index to $j' \to (j'+1)/2 = j$. Note that it was implicitly necessary that L is even which is the case for periodic boundary conditions.

Next, we utilize the Fourier transform of the operators to convert them into momentum space. The Fourier transform is given by

$$a_j^{\dagger} = \sqrt{\frac{2}{L}} \sum_{k'} e^{-ik'j} a_{k'}^{\dagger} \quad \text{and} \quad b_j^{\dagger} = \sqrt{\frac{2}{L}} \sum_{k'} e^{-ik'j} b_{k'}^{\dagger},$$

where the momenta are $k' = 4\pi k/L$ with integer $k \in [0, L/2 - 1]$. Afterwards, we always combine two exponential functions and the sums of the site index j to obtain a

Kronecker delta. This is then evaluated using the momentum sums. Thus, we obtain

$$\begin{aligned}
H &= -t\sum_{\sigma}\sum_{j=1}^{L/2} a^{\dagger}_{j\sigma}b_{j\sigma} - t'\sum_{\sigma}\sum_{j=1}^{L/2} b^{\dagger}_{j\sigma}a_{j+1\sigma} + \text{h.c.} \\
&= -t\frac{2}{L}\sum_{\sigma,k_1',k_2'}\sum_{j=1}^{L/2} e^{-ij(k_1'-k_2')}a^{\dagger}_{k_1'\sigma}b_{k_2'\sigma} - t'\frac{2}{L}\sum_{\sigma,k_1',k_2'}\sum_{j=1}^{L/2} e^{-ij(k_1'-k_2')}e^{ik'}b^{\dagger}_{k_1'\sigma}a_{k_2'\sigma} + \text{h.c.} \\
&= -t\sum_{\sigma,k_1',k_2'}\delta_{k_1',k_2'}a^{\dagger}_{k_1'\sigma}b_{k_2'\sigma} - t'\sum_{\sigma,k_1',k_2'}\delta_{k_1',k_2'}e^{ik_2'}b^{\dagger}_{k_1'\sigma}a_{k_2'\sigma} + \text{h.c.} \\
&= -t\sum_{\sigma,k_1'}a^{\dagger}_{k_1'\sigma}b_{k_1'\sigma} - t'\sum_{\sigma,k_1'}e^{ik_1'}b^{\dagger}_{k_1'\sigma}a_{k_1'\sigma} + \text{h.c.} \\
&= \sum_{\sigma,k_1'}(-t - t'e^{-ik_1'})a^{\dagger}_{k_1'\sigma}b_{k_1'\sigma} + \sum_{\sigma,k_1'}(-t - t'e^{ik_1'})b^{\dagger}_{k_1'\sigma}a_{k_1'\sigma} \\
&= \sum_{\sigma,k_1'}\begin{pmatrix} a^{\dagger}_{k_1'\sigma} & b^{\dagger}_{k_1'\sigma}\end{pmatrix}\begin{pmatrix} 0 & -t - t'e^{-ik_1'} \\ -t - t'e^{ik_1'} & 0\end{pmatrix}\begin{pmatrix} a_{k_1'\sigma} \\ b_{k_1'\sigma}\end{pmatrix}
\end{aligned}$$

where we have transformed into matrix notation in the last step. The resulting matrix is now easily diagonalized using the characteristic polynomial. Thus, the eigenvalues are

$$\lambda_{\pm} = \pm\sqrt{t^2 + t'^2 + 2tt'\cos(k')}.$$

So for each momentum sector we obtain two energy states. The spin sectors are degenerate, hence all eigenvalues are the same for the $S_z = 1/2$ and $S_z = -1/2$ sector.

Now let us considered many particle states. We construct these by following the simple procedure. Firstly, the spin S_z component needs to be the sum of the single particle S_z components. Furthermore, to obtain the correct momentum we also add the momenta of the single particle states. Note however that in contrast to the spin, the momentum is cyclic. Lastly, each single particle state is only inherited once in one many particle state.

B The Pseudospin η-Pair Symmetry

In this section we cover more details about the η-pair symmetry. For this, we summarize ideas of [MRB20; MBR22] and [Ess+05]. First, we introduce and elaborate the definitions of the η-pair operators and their symmetry. Then we discuss for this symmetry the definition of a spectrum generating algebra and its consequences. In the end, we connect the η-pair symmetry with the particle-hole symmetry by considering the Shiba transform.

B.1 General Definition

The foundation of this symmetry is given by the ladder operators $\eta_\pm$ that are defined as

$$\eta_+ = \sum_{j=1}^{L} (-1)^{j+1} c_{j\uparrow}^\dagger c_{j\downarrow}^\dagger \quad \text{and} \quad \eta_- = \eta_+^\dagger = \sum_{j=1}^{L} (-1)^{j+1} c_{j\downarrow} c_{j\uparrow} \tag{B.1}$$

where $c_{j\sigma}^\dagger$ and $c_{j\sigma}$ are the fermionic creation and annihilation operators. We may interpret the η_+ as an operator creating a pair state consisting of a spin up and a spin down particle on the same site. Before further elaborating this notion let us construct the algebra first. As a reminder, for the spin SU(2) algebra the defining commutation relations are given by

$$[S_z, S_\pm] = \pm S_\pm \quad \text{and} \quad [S_+, S_-] = 2S_z \tag{B.2}$$

where $S_\pm$ are the ladder operators and S_z the spin z-component. Using the second commutation relation we try to find a similar operator η_z for the η-pair ladder operators. This yields

$$\begin{aligned}
[\eta_+, \eta_-] &= \sum_{j,l} (-1)^{j+1} (-1)^{l+1} \left[c_{j\uparrow}^\dagger c_{j\downarrow}^\dagger, c_{l\downarrow} c_{l\uparrow} \right] \\
&= \sum_{j,l} (-1)^{j+1} (-1)^{l+1} \delta_{j,l} \left(c_{j\uparrow}^\dagger c_{l\uparrow} - c_{l\downarrow} c_{j\downarrow}^\dagger \right) \\
&= \sum_{j} \left(c_{j\uparrow}^\dagger c_{j\uparrow} + c_{j\downarrow}^\dagger c_{j\downarrow} - 1 \right) \\
&= N - L = 2\eta_z.
\end{aligned}$$

With this we define

$$\eta_z = \frac{1}{2}(N - L) \tag{B.3}$$

and we indeed find that $[\eta_z, \eta_\pm] = \pm\eta_\pm$. Note that here N denotes the particle number operator. Hence, similar to the spin algebra these operators generate an SU(2) algebra and are sometimes referred to as a pseudospin. We also define the respective Casimir operator similar to the spin algebra with

$$\eta^2 = \frac{1}{2}(\eta_+\eta_- + \eta_-\eta_+) + (\eta_z)^2 \tag{B.4}$$

that commutes with all other η operators.

Furthermore, we are going into more detail about the meaning of the operators. As discussed, the ladder operators can be understood as a creation or annihilation of a pair state. For a system with $L = 4$, this would take the form

$$\eta_+ |0\rangle = |1000|1000\rangle - |0100|0100\rangle + |0010|0010\rangle - |0001|0001\rangle \tag{B.5}$$

using the notation introduced in equation (3.1). This state has some interesting features. First, we note that it has a kinetic (hopping) energy of zero. The hoppings of two consecutive states in the superposition cancel because of the relative minus signs. This is not broken by the alternating hopping of the dimerized model. As a consequence, the only contribution to the energy is given by the interaction U,

$$H_{FH}\eta_+ |0\rangle = H_{dim}\eta_+ |0\rangle = U\eta_+ |0\rangle . \tag{B.6}$$

Furthermore, let us consider the pair state under translation and reflection. Acting with a translation T on it yields the eigenvalue -1 corresponding to a momentum of $k' = \pi$. For the dimerized model with the translation T_2 we find the eigenvalue 1 corresponding to $k' = 0$. Moreover, upon reflection at a bond, the parity of the pair state is $p = -1$. It is easy to verify this for the $L = 4$ example in equation (B.5).

The other two operators η_z and η^2 are similarly related as in the spin algebra. We denote the eigenvalues of η_z with $\tilde{n}$ and of η^2 with ξ. For a fixed ξ only values of $\tilde{n} \in \{-\xi, -\xi + 1, \ldots \xi - 1, \xi\}$ are possible. Acting with a ladder operator on an eigenstate $|\xi, \tilde{n}\rangle$ yields

$$\eta_\pm |\xi, \tilde{n}\rangle = |\xi, \tilde{n} \pm 1\rangle \tag{B.7}$$

if $\tilde{n} \pm 1$ is in the valid range. As an example, consider a fixed ξ and $\tilde{n} = -\xi$. Acting with η_- on such a state will yield zero. This corresponds to no pair state existing yet. By acting with η_+ on such a state we create pair states and increase $\tilde{n}$. This makes sense as $\tilde{n} + 1$ corresponds to adding two particles, in this case the pair. This is possible until we reach $\tilde{n} = \xi$. Then, again trying to add another pair state is not possible. Hence, states in a ξ sector are only able to contain up to $2\xi + 1$ pair states and $\tilde{n}$ corresponds to the number of pair states present for a fixed ξ.

There is one more difficulty that lies in the combination of the spin and η-pair pseudospin. Considering equation (B.3) for an arbitrary s one might expect to find the maximal value for $\tilde{n}$ of $N = 2L$ resulting in $\tilde{n}_{max} = L/2$. For $s \neq 0$ this state is not valid and as a consequence $\tilde{n}_{max} = L/2 - s$. We could also argue the other way around that for $N = 2L$ it is given that $m = s = 0$ which seems more intuitive as we are more used to working with the spin.

Now let us turn towards the symmetry aspect of the η-pairs. The two operators η_z and η^2 commute with both the Fermi Hubbard Hamiltonian as well as the dimerized Hubbard Hamiltonian. Moreover, the two operators also commute with the spin operators S_z and S^2 as well as the translation and reflection. Therefore, they introduce two more conserved quantities ξ for η^2 and $\tilde{n}$ for η_z. Note that the conservation of particle number N can be covered using the U(1) gauge symmetry but is also included in the η_z symmetry.

B.2 Spectrum Generating Algebra Structure

One major difference between the spin and pseudospin algebra lies within the commutation of the ladder operators. For the spin algebra we find

$$[H, S_\pm] = 0 \tag{B.8}$$

while for the pseudospin the commutation rule is

$$[H, \eta_\pm] = \pm U \eta_\pm. \tag{B.9}$$

An algebra with such a commutation relation can be referred to as a spectrum generating algebra. The last commutation can be understood intuitively. The $\eta_\pm$ create pair states having no kinetic energy and only a contribution of U. Hence, commuting the Hamiltonian with such a ladder operator should yield a difference of U. Furthermore, while equation (B.8) yields a degeneracy in the m sectors, equation (B.9) does not yields these degeneracies.

However, we find another interesting structure. Applying η_+ acting on a state $|\xi, \tilde{n}\rangle$ with energy $E_{\xi,\tilde{n}}$ yields us the state $|\xi, \tilde{n}+1\rangle$ with energy $E_{\xi,\tilde{n}+1} = U + E_{\xi,\tilde{n}}$. Hence, for an initial state φ we find a set of states $\{\varphi, \eta_+\varphi, \ldots, (\eta_+)^M\varphi\}$ with corresponding energies $\{E_\varphi, U + E_\varphi, \ldots, MU + E_\varphi\}$ which are called towers. If it is possible to find such a tower in a final symmetry subsector, it may result in quantum scars [MRB20; MBR22]. In our case, each state of such a tower lies in a different $\tilde{n}$ subsector and, therefore, this does not affect us. Still, this set of equidistant energies is an interesting phenomenon.

For instance, when considering the properties of the level statistics, this structure of equidistant energies is a useful feature. As discussed, we do not find degeneracies between the $\tilde{n}$ sectors for fixed ξ, but the spectrum shifted by U. When calculating the level spacings this shift cancels. As a consequence, different $\tilde{n}$ sectors yield the exact same distribution of ratios.

B.3 Shiba Transform and Connection to the Particle-Hole Symmetry

In section B.1 we have introduced the η-pair symmetry by constructing an SU(2) algebra on the foundation of the ladder operators $\eta_\pm$. There is also a different approach using the Shiba transform and the spin symmetry [Ess+05].

We can define the Shiba transform by the action on a creation/annihilation operator by

$$F_\sigma c_{j\sigma} F_\sigma = (-1)^j c^\dagger_{j\sigma} \tag{B.10}$$

or in an explicit manner with

$$F_\sigma = (c^\dagger_{L\sigma} - c_{L\sigma})(c^\dagger_{L-1\sigma} + c_{L-1\sigma}) \cdots (c^\dagger_{1\sigma} + c_{1\sigma}). \tag{B.11}$$

Note that the transformation is spin dependent. This is also the major difference to the definition of the particle-hole symmetry in equation (2.22). We can write equivalently

$$F = F_\uparrow F_\downarrow S_{flip} \tag{B.12}$$

where S_{flip} denotes the spin flip necessary to preserve the m conservation for the particle-hole symmetry F. Therefore, the Shiba transform can be understood as a particle-hole transformation in only one spin sector.

We can now apply the Shiba transform on the operators of the spin algebra S_z, S^2 and $S_\pm$ to obtain

$$F_\downarrow S_z (F_\downarrow)^\dagger = \eta_z, \quad F_\downarrow S_\pm (F_\downarrow)^\dagger = -\eta_\pm \quad \text{and} \quad F_\downarrow S^2 (F_\downarrow)^\dagger = \eta^2. \tag{B.13}$$

Hence, the Shiba transform poses a link between the spin algebra and the η-pair algebra.

All of this suggests that the particle-hole symmetry and the η-pair symmetry are related. To elaborate this, we consider a sector other than half filling, without loss of generality with $N < L$. Applying the particle-hole symmetry to the states in this sector projects onto the sector with particle number $2L - N$. We can reach the same sector using the ladder operator η_+ by applying it $(L - N)/2$ times. We have already discussed that we then expect a shift in the energies of the sector by $U(L - N)/2$. Calculating the commutation relations of the Hamiltonian and the particle-hole operator F yields the same result. Thus, at least beyond half filling, the action of the particle-hole operator is already included in the η-pair symmetry.

However, we already know that the particle-hole symmetry is not present for other cases than half filling. Hence, we want to superficially discuss the half filling case. First, note that for the corresponding sectors $\tilde{n} = 0$ and $\xi \in \{0, \ldots, L/2 - s\}$. All sectors with $\xi \neq 0$ are equivalent to other filling's sectors not exhibiting the particle-hole symmetry in the first place. Therefore, we restrict our discussion to the sector with $\xi = 0$. For a state $|\phi\rangle$ in this sector we know that $\eta_\pm |\phi\rangle = 0$. Now various states in position basis are part of the superposition in $|\phi\rangle$. For instance, we find states where one particle is located on each site, either spin up or spin down. Applying $\eta_\pm$ to such a state becomes zero, while the particle-hole operator F yields the same state again. Therefore, for these states F is already included.

If there is a state $|s\rangle$ in the superposition containing two particles at a site l, there also has to be an empty site m. For $\eta_\pm |\phi\rangle = 0$ it is necessary that the superposition in $|\phi\rangle$ also contains a state where site m contains two particles and site l none. Otherwise $\eta_\pm$ would create a state that cannot be cancelled. However, this is again the state we would obtain by applying F to $|s\rangle$. This argument can be extended inductively for more sites containing two particles. As a consequence the operator F projects on the same state $|\phi\rangle$ again.

Performing this calculation rigorously yields that the particle-hole symmetry is already included in the η-pair symmetry even for half filling.

C Details on the Implementation of the Spatial Symmetries

The implementation of the spatial symmetries was briefly discussed in section 3.2.2. This appendix is dedicated to its details. First, we are going to discuss the translation symmetries with its specialities. Then, we continue this discussion for the reflection symmetry. Again note that for the overall ideas about the exact diagonalization we refer to [WF08].

C.1 Translation Symmetry

The two-site translation projects the creation/annihilation operator on site j to site $j+2$

$$T_2 c_{j\sigma} (T_2)^\dagger = c_{j+2\sigma}. \tag{C.1}$$

Thus, the overall action of T_2 on a state is given by

$$|n_{1\uparrow} \dots n_{L\uparrow} | n_{1\downarrow} \dots n_{L\downarrow}\rangle \longrightarrow |n_{L-1\uparrow} n_{L\uparrow} n_{1\uparrow} \dots n_{L-2\uparrow} | n_{L-1\downarrow} n_{L\downarrow} n_{1\downarrow} \dots n_{L-2\downarrow}\rangle \tag{C.2}$$

where we use the notation introduced in equation (3.1). This notation defined an order for the creation operators which, in general, is destroyed by acting with a translation. Recall that this ordering is given by

$$\begin{aligned} |n_{1\uparrow} n_{2\uparrow} \dots n_{L\uparrow} | n_{1\downarrow} n_{2\downarrow} \dots n_{L\downarrow}\rangle &= \prod_{i\in I} c^\dagger_{i\uparrow} \prod_{j\in J} c^\dagger_{j\downarrow} |0\rangle \\ &= (c^\dagger_{1\uparrow})^{n_{1\uparrow}} \cdots (c^\dagger_{L\uparrow})^{n_{L\uparrow}} (c^\dagger_{1\downarrow})^{n_{1\downarrow}} \cdots (c^\dagger_{L\downarrow})^{n_{L\downarrow}} |0\rangle \end{aligned}$$

where the operators with last sites act first. To remain consistent we have to anti-commute all operators such that the defined order is restored. This process does not exclude the emergence of signs which need to be considered.

The conditions for such a sign to appear can be derived. Note, that due to our ordering we can consider the spin chains individually. First of all, a sign can only emerge if at least one particle is translated from the last two sites to the first two sites. Otherwise, the order of the creation operators is preserved. For now, we consider only the translation by one site with a particle located at the last site. Then we obtain

$$\begin{aligned} \hat{T} \, |n_{1\sigma} \dots n_{L-1\sigma} 1\rangle &= \hat{T} \prod_{i\in I\setminus L} c^\dagger_{i\sigma} c^\dagger_{L\sigma} |0\rangle \\ &= \prod_{i\in I\setminus L} c^\dagger_{i+1\sigma} c^\dagger_{1\sigma} |0\rangle \\ &= (-1)^{N_\sigma - 1} c^\dagger_{1\sigma} \prod_{i\in I\setminus L} c^\dagger_{i+1\sigma} |0\rangle \\ &= (-1)^{N_\sigma - 1} \, |1 n_{1\sigma} \dots n_{L-1\sigma}\rangle \end{aligned}$$

where $I \setminus L$ is the set of all indices with a particle excluding site L. We can observe that for even sector particle number N_σ the sign appears, while for an odd number we obtain no sign.

For the two-site translation we just combine twice the translation T. Hence, if two or no particles are located on the last two sites, no sign can arise. For only one particle a sign emerges for even sector particle number N_σ. After considering each spin chains individually the two factors have to be multiplied to obtain the final sign.

Next we consider some examples.

- $|0011|1010\rangle$: In both spin sectors we find an even number of particles. For the spin up part, two particles are located at the last two sites. Therefore, we obtain no sign in the spin up regime. However, for spin down we find only one particle, thus, yielding a sign. In total, the application of T_2 would yield a factor of -1.

- $|1101|1010\rangle$: Even though we find only one particle on the last two sites in both spin sectors, only the spin down sign contributes as $N_\uparrow$ is odd. In total a factor of -1 emerges.

- $|1100|1000\rangle$: No particle is located on the last two sites. Hence, no sign emerges.

These signs need to be considered when constructing the eigenstates. For this we want to superpose all states which are related by translations T_2. This can be represented using projection operators. The projection operator of the translation symmetry is given by

$$P_t(k) = \frac{2}{L} \sum_{l=1}^{L/2} e^{ilk} T_2^l. \tag{C.3}$$

This operator sums all possible translations of a representative $|s\rangle$ while providing the correct coefficients for a momentum k. As discussed in section 3.2.2 it suffices to memorize the representatives and the coefficients of the superposition.

We are now going to discuss the composition of the coefficients. Besides the e^{ijk} factor of the projection operator we also have to include the correct sign from the translation. Moreover, a proper normalization is necessary. If each translation of the representative $|s\rangle$ is unique, the normalization factor is given by $\mathcal{N} = \sqrt{L/2}$. For other cases, if the initial state $|s\rangle$ is obtained after less than $L/2$ translations, the normalization needs to be adapted. In this case the superposition is given by less than $L/2$ states, Note that the normalization can only be $\sqrt{L/(2j)}$ where j is an integer.

This induces another problem. For some momenta k the projection $P_t(k)\,|s\rangle$ cancels. The exact momenta depend on the number of translation necessary to find $|s\rangle$ and the sign this translation yields. As an example, consider the state $|1010|1010\rangle$ which is obtained after $L/4$ translations with no sign emerging from the translation. Thus, the projection with $k' = \pi$ will cancel. However, if we obtain an additional sign with the translation as it is the case for $|1010|0000\rangle$, the projection cancels itself for $k' = 0$.

Hence, constructing the states and especially calculating the correct coefficients is non-trivial. We now give a short summary on how to implement such a construction. We start by going through the list of available states at this point. Each state is translated until it reaches an already found representative or itself. If it reaches and does not cancel itself due to the translation sign, it is memorized as a representative. Otherwise the coefficient can be calculated by using the number of translation necessary and the signs of the translation. This coefficient does not include the normalization. This can be memorized parallelly counting the number of states assigned to a representative. If all available states are considered we have a list of representative with their respective norms as well as a list of all coefficients.

Note that in the case of the routine written for this thesis, the coefficients were memorized in a more general manner such that they could be used for an arbitrary k sector with fixed L, N, m. However, the general idea remains the same.

C.2 Reflection Symmetry

Next, we turn our attention towards the reflection symmetry. We use the definition for the reflection at a bond given by

$$R_b c_{j\sigma} R_b^\dagger = c_{L+1-j\sigma} \tag{C.4}$$

where we omit the subscript for the sake of simplicity. Again the reflection may destroy the order of the creation operators yielding a sign. This is always the case if $(N_\sigma^2 - N_\sigma)/2$ is odd. To check this consider once more the spin chains individually and find

$$\begin{aligned}\hat{R} \left| n_{1\sigma} \dots n_{L\sigma} \right\rangle &= \hat{R} \prod_{i \in I} c_{i\sigma}^\dagger \left| 0 \right\rangle \\ &= \prod_{i \in I} c_{L+1-i,\sigma}^\dagger \left| 0 \right\rangle .\end{aligned}$$

To place the operator with the lowest index on left again we obtain a sign $(-1)^{N-1}$, for the next one $(-1)^{N-2}$ and so on. Thus, in the end the sign we obtain is $(-1)^{\sum_{j=1}^{N} N-j}$. The exponent can be calculated with

$$\begin{aligned}\sum_{j=1}^{N} N - j &= N^2 - \sum_{j=1}^{N} j \\ &= N^2 - \frac{N(N+1)}{2} \\ &= \frac{N^2 - N}{2}\end{aligned}$$

which yields the claim. Again the total sign is the multiplication of the spin sector signs.

The overall process of constructing the basis of the reflection symmetry does not differ much from the translation symmetry. An advantage is that the projection

$$P_r(p) = \frac{1}{2}(1 + pR) \tag{C.5}$$

is a superposition of only two states with $p \in \{\pm 1\}$. Therefore, the coefficients do not contain any exponentials and are composed of the parity p, the reflection sign factor and the normalization. Note, that self-reflective states again pose special cases where the normalization has to be adapted.

For the simultaneous construction of both translation and reflection symmetry's eigenbasis, the procedure is again similar. The major difference is that the states do not only need to be checked whether they are translational wise related but also by reflection. The calculation of the coefficients has to be done very carefully to not omit any factor at this point. To memorize the coefficients more generally more work has to put into this procedure. However, the general idea is again captured by the given description.

References

[Aba+19] Dmitry A. Abanin et al. "Colloquium: Many-body localization, thermalization, and entanglement". In: *Rev. Mod. Phys.* 91 (2 May 2019), p. 021001. DOI: 10.1103/RevModPhys.91.021001. URL: https://link.aps.org/doi/10.1103/RevModPhys.91.021001.

[Arn89] V. I. Arnold. *Mathematical Methods of Classical Mechanics*. New York: Springer New York, NY, 1989.

[Ata+13] Y. Y. Atas et al. "Distribution of the Ratio of Consecutive Level Spacings in Random Matrix Ensembles". In: *Phys. Rev. Lett.* 110 (8 Feb. 2013), p. 084101. DOI: 10.1103/PhysRevLett.110.084101. URL: https://link.aps.org/doi/10.1103/PhysRevLett.110.084101.

[BGS84] O. Bohigas, M. J. Giannoni, and C. Schmit. "Characterization of Chaotic Quantum Spectra and Universality of Level Fluctuation Laws". In: *Phys. Rev. Lett.* 52 (1 Jan. 1984), pp. 1–4. DOI: 10.1103/PhysRevLett.52.1. URL: https://link.aps.org/doi/10.1103/PhysRevLett.52.1.

[BT77] M. V. Berry and M. Tabor. "Level clustering in the regular spectrum". In: *Proc. R. Soc. Lond.* 356 (1686 Sept. 1977), pp. 375–394. DOI: 10.1098/rspa.1977.0140. URL: https://doi.org/10.1098/rspa.1977.0140.

[Bun79] L. A. Bunimovich. "On the ergodic properties of nowhere dispersing billiards". In: *Communications in Mathematical Physics* 65 (3 Oct. 1979), pp. 295–312. DOI: 10.1007/BF01197884. URL: https://doi.org/10.1007/BF01197884.

[CM11] Jean-Sébastien Caux and Jorn Mossel. "Remarks on the notion of quantum integrability". In: *Journal of Statistical Mechanics: Theory and Experiment* 2011.02 (Feb. 2011), P02023. DOI: 10.1088/1742-5468/2011/02/p02023. URL: https://doi.org/10.1088%2F1742-5468%2F2011%2F02%2Fp02023.

[DAl+16] Luca D'Alessio et al. "From quantum chaos and eigenstate thermalization to statistical mechanics and thermodynamics". In: *Advances in Physics* 65.3 (May 2016), pp. 239–362. DOI: 10.1080/00018732.2016.1198134. URL: https://doi.org/10.1080%2F00018732.2016.1198134.

[De +22] Jeannette De Marco et al. "Level statistics of the one-dimensional ionic Hubbard model". In: *Phys. Rev. Res.* 4 (3 Aug. 2022), p. 033119. DOI: 10.1103/PhysRevResearch.4.033119. URL: https://link.aps.org/doi/10.1103/PhysRevResearch.4.033119.

[Deu91] J. M. Deutsch. "Quantum statistical mechanics in a closed system". In: *Phys. Rev. A* 43 (4 Feb. 1991), pp. 2046–2049. DOI: 10.1103/PhysRevA.43.2046. URL: https://link.aps.org/doi/10.1103/PhysRevA.43.2046.

[Ess+05] F.H.L. Essler et al. *The One-Dimensional Hubbard Model*. Cambridge: Cambridge University Press, 2005.

[Ess10] Tilman Esslinger. "Fermi-Hubbard Physics with Atoms in an Optical Lattice". In: *Annual Review of Condensed Matter Physics* 1.1 (Aug. 2010), pp. 129–152. DOI: 10.1146/annurev-conmatphys-070909-104059. URL: https://doi.org/10.1146%2Fannurev-conmatphys-070909-104059.

[Gir+22] Olivier Giraud et al. "Probing Symmetries of Quantum Many-Body Systems through Gap Ratio Statistics". In: *Phys. Rev. X* 12 (1 Jan. 2022), p. 011006. DOI: 10.1103/PhysRevX.12.011006. URL: https://link.aps.org/doi/10.1103/PhysRevX.12.011006.

[GMW98] Thomas Guhr, Axel Müller–Groeling, and Hans A. Weidenmüller. "Random-matrix theories in quantum physics: common concepts". In: *Physics Reports* 299.4 (1998), pp. 189–425. ISSN: 0370-1573. DOI: https://doi.org/10.1016/S0370-1573(97)00088-4. URL: https://www.sciencedirect.com/science/article/pii/S0370157397000884.

[Góm+02] J. M. G. Gómez et al. "Misleading signatures of quantum chaos". In: *Phys. Rev. E* 66 (3 Sept. 2002), p. 036209. DOI: 10.1103/PhysRevE.66.036209. URL: https://link.aps.org/doi/10.1103/PhysRevE.66.036209.

[HJ20] Abolfath Hosseinzadeh and Seyed Akbar Jafari. "Quantum Integrability of 1D Ionic Hubbard Model". In: *Annalen der Physik* 532.3 (2020), p. 1900601. DOI: https://doi.org/10.1002/andp.201900601. eprint: https://onlinelibrary.wiley.com/doi/pdf/10.1002/andp.201900601. URL: https://onlinelibrary.wiley.com/doi/abs/10.1002/andp.201900601.

[LW68] Elliott H. Lieb and F. Y. Wu. "Absence of Mott Transition in an Exact Solution of the Short-Range, One-Band Model in One Dimension". In: *Phys. Rev. Lett.* 20 (25 June 1968), pp. 1445–1448. DOI: 10.1103/PhysRevLett.20.1445. URL: https://link.aps.org/doi/10.1103/PhysRevLett.20.1445.

[MBR22] Sanjay Moudgalya, B Andrei Bernevig, and Nicolas Regnault. "Quantum many-body scars and Hilbert space fragmentation: a review of exact results". In: *Reports on Progress in Physics* 85.8 (July 2022), p. 086501. DOI: 10.1088/1361-6633/ac73a0. URL: https://doi.org/10.1088%2F1361-6633%2Fac73a0.

[Meh04] M. L. Mehta. *Random Matrices*. Amsterdam: Elsevier Academic Press, 2004.

[MRB20] Sanjay Moudgalya, Nicolas Regnault, and B. Andrei Bernevig. "Eta-Pairing in Hubbard Models: From Spectrum Generating Algebras to Quantum Many-Body Scars". In: (2020). DOI: 10.48550/ARXIV.2004.13727. URL: https://arxiv.org/abs/2004.13727.

[Nak+16] Shuta Nakajima et al. "Topological Thouless pumping of ultracold fermions". In: *Nature Physics* 12.4 (Jan. 2016), pp. 296–300. DOI: 10.1038/nphys3622. URL: https://doi.org/10.1038%2Fnphys3622.

[NH15] Rahul Nandkishore and David A. Huse. "Many-Body Localization and Thermalization in Quantum Statistical Mechanics". In: *Annual Review of Condensed Matter Physics* 6.1 (Mar. 2015), pp. 15–38. DOI: 10.1146/annurev-conmatphys-031214-014726. URL: https://doi.org/10.1146%2Fannurev-conmatphys-031214-014726.

[OH07] Vadim Oganesyan and David A. Huse. "Localization of interacting fermions at high temperature". In: *Phys. Rev. B* 75 (15 Apr. 2007), p. 155111. DOI: 10.1103/PhysRevB.75.155111. URL: https://link.aps.org/doi/10.1103/PhysRevB.75.155111.

[PBG89] A Pandey, O Bohigas, and M J Giannoni. "Level repulsion in the spectrum of two-dimensional harmonic oscillators". In: *Journal of Physics A: Mathematical and General* 22.18 (Sept. 1989), p. 4083. DOI: 10.1088/0305-4470/22/18/039. URL: https://dx.doi.org/10.1088/0305-4470/22/18/039.

[Poi+93] D Poilblanc et al. "Poisson vs. GOE Statistics in Integrable and Non-Integrable Quantum Hamiltonians". In: *Europhysics Letters (EPL)* 22.7 (June 1993), pp. 537–542. DOI: 10.1209/0295-5075/22/7/010. URL: https://doi.org/10.1209%2F0295-5075%2F22%2F7%2F010.

[PR91] Akhilesh Pandey and Ramakrishna Ramaswamy. "Level spacings for harmonic-oscillator systems". In: *Phys. Rev. A* 43 (8 Apr. 1991), pp. 4237–4243. DOI: 10.1103/PhysRevA.43.4237. URL: https://link.aps.org/doi/10.1103/PhysRevA.43.4237.

[RDO08] Marcos Rigol, Vanja Dunjko, and Maxim Olshanii. "Thermalization and its mechanism for generic isolated quantum systems". In: *Nature* 452.7189 (Apr. 2008), pp. 854–858. DOI: 10.1038/nature06838. URL: https://doi.org/10.1038%2Fnature06838.

[Ret22] Ana L Retore. "Introduction to classical and quantum integrability". In: *Journal of Physics A: Mathematical and Theoretical* 55.17 (Apr. 2022), p. 173001. DOI: 10.1088/1751-8121/ac5a8e. URL: https://doi.org/10.1088%2F1751-8121%2Fac5a8e.

[Rig09] Marcos Rigol. "Breakdown of Thermalization in Finite One-Dimensional Systems". In: *Phys. Rev. Lett.* 103 (10 Sept. 2009), p. 100403. DOI: 10.1103/PhysRevLett.103.100403. URL: https://link.aps.org/doi/10.1103/PhysRevLett.103.100403.

[RS12] Marcos Rigol and Mark Srednicki. "Alternatives to Eigenstate Thermalization". In: *Physical Review Letters* 108.11 (Mar. 2012). DOI: 10.1103/physrevlett.108.110601. URL: https://doi.org/10.1103%2Fphysrevlett.108.110601.

[San10] Anders W. Sandvik. "Computational Studies of Quantum Spin Systems". In: *AIP Conference Proceedings* 1297.1 (2010), pp. 135–338. DOI: 10.1063/1.3518900. eprint: https://aip.scitation.org/doi/pdf/10.1063/1.3518900. URL: https://aip.scitation.org/doi/abs/10.1063/1.3518900.

[Sin70] Yakov G Sinai. "Dynamical systems with elastic reflections". In: *Russian Mathematical Surveys* 25.2 (Apr. 1970), p. 137. DOI: 10.1070/RM1970v025n02ABEH003794. URL: https://dx.doi.org/10.1070/RM1970v025n02ABEH003794.

[Sre94] Mark Srednicki. "Chaos and quantum thermalization". In: *Physical Review E* 50.2 (Aug. 1994), pp. 888–901. DOI: 10.1103/physreve.50.888. URL: https://doi.org/10.1103%2Fphysreve.50.888.

[Sre99] Mark Srednicki. "The approach to thermal equilibrium in quantized chaotic systems". In: *Journal of Physics A: Mathematical and General* 32.7 (Feb. 1999), p. 1163. DOI: 10.1088/0305-4470/32/7/007. URL: https://dx.doi.org/10.1088/0305-4470/32/7/007.

[Wei92] Stefan Weigert. "The problem of quantum integrability". In: *Physica D: Nonlinear Phenomena* 56.1 (1992), pp. 107–119. ISSN: 0167-2789. DOI: https://doi.org/10.1016/0167-2789(92)90053-P. URL: https://www.sciencedirect.com/science/article/pii/016727899290053P.

[WF08] Alexander Weiße and Holger Fehske. "Exact Diagonalization Techniques". In: *Computational Many-Particle Physics*. Ed. by H. Fehske, R. Schneider, and A. Weiße. Berlin, Heidelberg: Springer Berlin Heidelberg, 2008, pp. 529–544. ISBN: 978-3-540-74686-7. DOI: 10.1007/978-3-540-74686-7_18. URL: https://doi.org/10.1007/978-3-540-74686-7_18.

[Wig55] Eugene P. Wigner. "Characteristic Vectors of Bordered Matrices With Infinite Dimensions". In: *Annals of Mathematics* 62.3 (1955), pp. 548–564. ISSN: 0003486X. URL: http://www.jstor.org/stable/1970079 (visited on 02/20/2023).

[Wim22] Sandro Wimberger. *Nonlinear Dynamics and Quantum Chaos*. 2nd ed. Cham: Springer, 2022.